SUBARU DEEP SURVEY V. A CENSUS OF LYMAN BREAK GALAXIES AT $Z\simeq 4$ AND 5 IN THE SUBARU DEEP FIELDS: PHOTOMETRIC PROPERTIES¹

ABSTRACT

We investigate photometric properties of Lyman Break Galaxies (LBGs) at z = 3.5 - 5.2 based on large samples of 2,600 LBGs detected in deep ($i' \lesssim 27$) and wide-field (1,200 arcmin²) images taken in the Subaru Deep Field (SDF) and the Subaru/XMM Deep Field (SXDF) using broad band B, V, R, i', and z' filters. The selection criteria for the LBG samples are examined with 85 spectroscopically identified objects, and the completeness and contamination of the samples are estimated from Monte Carlo simulations based on a photometric-redshift catalog of the Hubble Deep Field-North. We find that these LBG samples are nearly rest-frame UV magnitude-limited samples, missing systematically only 10% of red high-z galaxies (in number) which are a dusty population with $E(B-V) \gtrsim 0.4$. We calculate luminosity functions of the LBGs with the estimated completeness and contamination, and find (i) that the number density of bright galaxies $(M_{1700} < -22$; corresponding to SFR $\gtrsim 100 h_{70}^{-2} M_{\odot} \mathrm{yr}^{-1}$ with extinction correction) decreases significantly from z = 4 to 5 and (ii) that the faint-end slope of the luminosity functions of LBGs may become steeper towards higher redshifts. We estimate dust extinction of $z \simeq 4$ LBGs with $M < M^*(\simeq -21)$ from UV-continuum slopes, and obtain $E(B-V) = 0.15 \pm 0.03$ as the mean value. The dust extinction remains constant with apparent luminosity, but increases with intrinsic (i.e., extinction-corrected) luminosity. We find no evolution in dust extinction between LBGs at z=3 and 4. We investigate the evolution of UV-luminosity density by integrating the luminosity functions of LBGs, and find that the UV-luminosity density at 1700Å, $\rho_{\rm UV}$ does not significantly change from z = 3 to z = 5, i.e., $\rho_{\rm UV}(z = 4)/\rho_{\rm UV}(z = 3) = 1.0 \pm 0.2$ and $\rho_{\rm UV}(z = 5)/\rho_{\rm UV}(z = 3) = 0.8 \pm 0.4$, thus the cosmic star-formation rate (SFR) density (with correction for dust extinction) remains constant within the error bars, or possibly a slight decline, from z=3 to z=5. We estimate the stellar mass density from the cosmic SFR thus obtained, and find that this stellar mass density is consistent with those derived directly from the stellar mass function at z=0-1, but exceeds those at $z\sim3$ by a factor of 3. We find that the ratio of the UV-luminosity density of Lyman α emitters (LAEs) to that of LBGs is $\simeq 60\%$ at $z \simeq 5$, and thus about a half of star formation probably occurs in LAEs at $z \simeq 5$. We obtain a constraint on the escape fraction of UV-ionizing photons (i.e., UV continuum in 900Å) produced by LBGs, $f_{\rm esc} \gtrsim 0.13$. This implies that the escape fraction of LBGs may be larger than that of star-forming galaxies at z=0.

Subject headings: cosmology: observations — galaxies: high-redshift — galaxies: evolution

1. INTRODUCTION

Formation history of galaxies is basically understood as a combination of two fundamental evolutionary processes, i.e., production of stars and accumulation of dark matter in the standard framework of galaxy formation which is the Cold Dark Matter (CDM) models. In order to investigate

the formation history of stars, one of the fundamental processes, many efforts have been made for searching for high-z galaxies up to $z\simeq 7$ (Hu et al. 2002; Kodaira et al. 2003). Very deep optical-to-near infrared imaging data such as the Hubble Deep Field-North (HDF-N) pioneered to detect high-z galaxies at $z\gtrsim 3$. The photometric-redshift (photo-z) method accurately identifies the redshifts of all

- ¹ Based on data collected at Subaru Telescope, which is operated by the National Astronomical Observatory of Japan.
- ² Department of Astronomy, School of Science, University of Tokyo, Tokyo 113-0033, Japan
- ³ Research center for the Early Universe, School of Science, University of Tokyo, Tokyo 113-0033, Japan
- ⁴ Subaru Telescope, National Astronomical Observatory, 650 N.A'ohoku Place, Hilo, HI 96720, USA
- 5 National Astronomical Observatory, Mitaka, Tokyo 181-8588, Japan
- ⁶ Institute of Astronomy, School of Science, University of Tokyo, Mitaka, Tokyo 181-0015, Japan
- ⁷ Department of Mathematical and Physical Sciences, Faculty of Science, Japan Women's University, Tokyo 112-8681, Japan
- ⁸ Department of Astronomy, Kyoto University, Sakyo-ku, Kyoto 606-8502
- ⁹ Department of Physics, University of Durham, South Road, Durham DH1 3LE, UK

¹⁰ Institute for Cosmic Ray Research, University of Tokyo, Kashiwa, Chiba 277-8582

high-z galaxies detected in the imaging data (e.g., Connolly et al. 1995; Gwyn & Hartwick 1996; Lanzetta, Yahil, & Fernandez-Soto 1996; Sawicki, Lin, & Yee 1997; Wang, Bahcall, & Turner 1998; Fernández-Soto, Lanzetta, & Yahil 1999; Benítez 2000; Fontana et al. 2000; Furusawa et al. 2000; Yahata et al. 2000; Massarotti, Iovino, Buzzoni, & Valls-Gabaud 2001; Rudnick et al. 2001). The photoz method has an advantage in identifying high-z galaxies with little systematic selection bias. However, the photoz method requires near-infrared images deep enough to detect faint high-z galaxies, as well as multi-band optical images. Thus, application of this technique is limited to small patches of the sky and to small numbers of galaxies at relatively low redshifts $(z \lesssim 3)$, due to the small fieldof-view of near-infrared imagers to date. On the other hand, the broad-band two color selection technique successfully identifies a large number of high-z galaxies detected only in optical bands, which is based on Lymanbreak (912Å) features redshifted to optical wavelengths (e.g., Steidel et al. 1996a,b; Madau et al. 1996; Lowenthal et al. 1997; Madau, Pozzetti, & Dickinson 1998; Steidel et al. 1999). High-z galaxies found by this method are called Lyman Break Galaxies, or LBGs. There are a few thousand of photometrically selected high-z $(2 \lesssim z \lesssim 4)$ galaxies, and about 1000 galaxies have been spectroscopically confirmed to be really located at $z \simeq 3$ (Steidel et al. 2003). The Lyman break technique is an ideal method for selecting a large number of high-z galaxies and for studying their general properties in a limited telescope time, since the method requires optical images in a few bandpasses. Furthermore, relative sensitivities in optical bands are better than those in near-infrared, and thus the Lyman break technique can identify higher-redshift $(z \gtrsim 4)$ galaxies than the photo-z method. A problem is that LBGs are generally UV-continuum bright galaxies, since they are identified by their strong Lyman breaks. It is thought that part of high-z galaxies escape from the Lyman break selection (e.g., Pascarelle, Windhorst, & Keel 1998; Dickinson 2000; Franx et al. 2003). Care is needed when we discuss properties of high-z galaxies using LBG samples.

Luminosity function (LF) of high-z galaxies are obtained to reveal the number density and the star-formation history of galaxies (e.g., Sawicki, Lin, & Yee 1997; Fernández-Soto, Lanzetta, & Yahil 1999; Furusawa et al. 2000; Poli et al. 2001; Kashikawa et al. 2003, hereafter SDS III). Steidel et al. (1999) find from their large LBG samples that the LF of LBGs at z=3 is well fitted by the Schechter function with a steep slope, $\alpha = -1.6$, down to $L \simeq 0.1L^*$, and that the UV-luminosity density derived by integrating the LF does not change from z=3 to z=4. Thus, the cosmic star-formation rate (SFR) estimated from the UVluminosity density does not significantly drop at $z \gtrsim 3$, which is different from the early report given by Madau et al. (1996) with HDF-N galaxies. A similar tendency in the cosmic SFR is also reported by Iwata et al. (2003) who derive the cosmic SFR at z = 5. Here, dust extinction is a critical issue in estimating the cosmic SFR from the UV-luminosity density.

Dust extinction of LBGs at $z \sim 3$ has been estimated by Steidel et al. (1999); Meurer, Heckman, & Calzetti (1999); Adelberger & Steidel (2000); Vijh, Witt, & Gordon (2003) (see also Calzetti 2001 for review) from UV

spectral slopes of LBGs. These authors show that the average (or median) dust extinction of LBGs at $z \sim 3$ is E(B-V) = 0.10 - 0.30, assuming the dust attenuation law of Calzetti, Kinney, & Storchi-Bergmann (1994) or Calzetti et al. (2000). Global spectral fitting from restframe UV to optical SEDs of LBGs at $z \sim 3$ supports this value (Sawicki & Yee 1998; Ouchi, Yamada, Kawai, & Ohta 1999; Shapley et al. 2001; Papovich, Dickinson, & Ferguson 2001). Near-infrared spectroscopy has also yielded similar values of dust extinction using the Balmer decrement (e.g., Pettini et al. 1998; Pettini et al. 2001, 2002). Since the dust-extinction correction for the UVluminosity ranges from a factor of 3 to 19 (presented in Vijh, Witt, & Gordon 2003 and references therein), it is a key to determine dust extinction accurately, so as to estimate the real SFR from the UV-luminosity density.

Measuring the stellar mass density (Brinchmann & Ellis 2000; Cole et al. 2001; Cohen 2002; Dickinson, Papovich, Ferguson, & Budavári 2003) is an independent check for cosmic SFR measurements, since the cosmic SFR is a derivative of the stellar mass density with respect to cosmic time. Dickinson, Papovich, Ferguson, & Budavári (2003) have derived the stellar mass density as a function of redshift up to z=3. They have found that the stellar mass density at z=3 is about 6% of that in the present epoch. However, the stellar mass density at z=3 they have estimated is less than that derived by integrating the cosmic SFR given by Steidel et al. (1999) (see Cole et al. 2001), where the cosmic SFR at high redshift $(5 \lesssim z \lesssim 7)$ is an extrapolation from measurements at $z \lesssim 4$. It is important to obtain accurate cosmic SFRs at $z \gtrsim 5$, and examine the cause of the discrepancy. High-z galaxies produce far-UV photons by their star-formation activities, and these far-UV photons contribute to the ionization of the Universe (e.g., Madau, Haardt, & Rees 1999). Thus, it is also important to measure the star-formation activity of high-z galaxies, and investigate the relationship between galaxies and the reionization of the Universe.

Observational studies of galaxies at $z \gtrsim 4$ were mainly based on data of the HDF-N and HDF-Sourth, both of which have only $\sim 4-5$ arcmin² (about $2'\times 2'$), corresponding to 4×4 Mpc² at z=4 (comoving units), i.e., cluster scales in the present-day universe. Surveys based on such a small area probably suffer from cosmic variance, i.e., spatial inhomogeneities of galaxy properties in the Universe. Cosmic variance is thought to be one of the major ambiguities in the measurements for luminosity function, luminosity density, and star-formation rate etc. Furthermore, small-field surveys do not provide clustering properties of galaxies on large scales which reflect properties of dark matter in galaxies, i.e., the other fundamental properties of galaxies.

In order to address the issues described above, we carry out deep and wide-field surveys for high-z galaxies with Subaru Prime Focus Camera (Suprime-Cam; Miyazaki et al. 2002), which is a wide-field ($34' \times 27'$) optical imager mounted on 8m Subaru. We made deep and wide-field imaging for two blank fields during the Guaranteed Time Observations (GTOs) of Suprime-Cam. One blank field is the Subaru Deep Field (SDF: $13^h24^m21.4^s, +27^\circ29'23''$ [J2000]; Maihara et al. 2001, hereafter SDS I; Ouchi et al. 2003a, hereafter SDS II;

SDS III; Shimasaku et al. 2003, hereafter SDS IV), and the other is the Subaru/XMM Deep Survey Field (SXDF: $2^{h}18^{m}00^{s}, -5^{\circ}00'00''[J2000];$ Sekiguchi et al. 2004 in preparation; see also Ouchi et al. 2001). These fields have little Galactic extinction and few bright stars over 1 deg^2 . Thus, these fields are suitable for studying high-z galaxies by deep observations with Suprime-Cam. These two blank fields, SDF and SXDF, have also been observed in two Subaru Observatory key projects. One is the SDF Project (Kashikawa et al.). The SDF project makes very deep observations for the SDF with Suprime-Cam, multislit spectrographs (e.g., Subaru/FOCAS: Kashikawa et al. 2002), and near-infrared cameras and spectrographs (e.g., Subaru/CISCO: Motohara et al. 2002), to study galaxy evolution at z=3-7. The area surveyed in the SDF project is about $0.2~\rm deg^2$, corresponding to one FoV of Suprime-Cam. The other is the Subaru/XMM Deep Survey (SXDS) Project (Sekiguchi et al.). The SXDS project is a wide-field multi-wavelength survey project. The field surveyed by Suprime-Cam in the SXDS project is about 1 deg² corresponding to 5 FoVs of Suprime-Cam. The SXDF is observed by many instruments in various wavelengths; radio with VLA, sub-millimeter with JCMT/SCUBA, infrared with SIRTF, near-infrared with UKIRT/WFCAM, optical with Subaru/Suprime-Cam and Subaru/FOCAS, ultra-violet with GALEX, and X-ray with XMM-Newton. This paper is based on the GTO data alone, which were taken in 2000 and 2001. Deeper images (3-10 hours for each band) have been obtained in the key projects, but reduction of them is still under way. 11

In this paper, we make large samples of LBGs at z=4and 5 with the deep and wide-field SDF+SXDF data (sections 2-3). We derive LFs of LBGs from the large LBG samples, and investigate the evolution of the LF (section 4). We calculate dust extinction for our LBGs at z = 4, and examine the evolution of dust extinction for star-forming galaxies over z = 0 - 4.5 (section 5). We calculate the UV-luminosity density of LBGs at z = 4 and 5, and investigate the cosmic SFR, the stellar mass density, and the escape fraction of far-UV photons for LBGs at z = 4 - 5 (section 6) where we use the dust extinction of LBGs obtained in the previous section. We present clustering properties of these LBGs in the companion paper (Ouchi et al. 2003c, hereafter SDS VI). In SDS VI, we combine the results of clustering properties with those of photometric properties shown in this paper using the CDM models, and give more detailed discussions.

Throughout this paper, magnitudes are in the AB system (Oke 1974; Fukugita, Shimasaku, & Ichikawa 1995). The values for the cosmological parameters adopted in this paper are: $(h, \Omega_m, \Omega_\Lambda, \Omega_b h^2) = (0.7, 0.3, 0.7, 0.02)$. These values are the same as those obtained from the latest CMB observations (Spergel et al. 2003).

2. OBSERVATIONS AND DATA REDUCTION

2.1. Observations

2.1.1. Imaging

During the commissioning runs of Suprime-Cam (November 2000 - November 2001), we carried out multi-band, deep and wide-field optical imaging in two blank fields. One is the Subaru Deep Field (SDF: $13^{h}24^{m}21.4^{s}, +27^{\circ}29'23''[J2000];$ SDS I), and the other is the Subaru/XMM Deep Field (SXDF: $2^{h}18^{m}00^{s}, -5^{\circ}12'00''[J2000]'$. The central 4 arcmin² region of the SDF has very deep J and K' data (SDS I). Although the central position of the SXDF is $2^{h}18^{m}00^{s}, -5^{\circ}00'00''$ (J2000) (Sekiguchi et al. 2004 in preparation), since some bright stars are located in the neighbor of the central position, we choose a southern part of the SXDF which is apart from the center by 12' for our observations. We observed these two blank fields in the B-, V-,R-, i'-, and z'-band filters which cover the whole optical-wavelength range (4000Å to 10000Å). Figure 1 shows the response of the filters used in these observations. The response includes atmospheric absorption, quantum efficiency, and transmittance of optical elements of Suprime-Cam.

The total exposure time ranges from 81 to 210 (40 to 177) minutes among the filters in the SDF (SXDF). The 3σ limiting magnitudes are i'=26.9 and i'=26.2 for the SDF and SXDF, respectively. During the observations, the seeing size varied from 0''.5 - 0''.9 and 0''.5 - 1''.0 for the SDF and SXDF. Table 1 summarizes the observations. We show pseudo-color images of the SDF and SXDF in Figure 2 and Figure 3. Although the FoV of Suprime-Cam is 918 arcmin² $(27' \times 34')$, only nine CCDs were installed (i.e., one CCD named w93c2 had not been installed; see Miyazaki et al. 2002 for positions of CCD chips) before March 2001. 12 In addition, one CCD named w67c1 installed in April 2001 showed strong fringes, and we do not use the data taken by this CCD. 13 We do not use, either, low-S/N regions located around the edge of the FoV, which are caused by dithering observations. After we reject these bad areas, the SXDF image has 653 arcmin² for all bandpasses. Similarly, the SDF image has 616 arcmin² for the B,V,i', and z' bands, and 543 arcmin² for the R band (see Table 1).

During the observations, we took images of photometric standard stars, SA92 and SA95 (Landolt 1992) in the B, V, and R bands, and spectrophotometric standard stars, SA95-42 and Hz44 (Oke 1990) in the i^\prime and z^\prime bands. These standard stars were observed a few times a night, when the night was thought to be photometric.

2.1.2. Spectroscopy

Spectroscopic redshift data are important to check our selection criteria for LBGs. We carried out spectroscopic follow-up observations of LBGs detected in our data with Faint Object Camera and Spectrograph (FOCAS; Kashikawa et al. 2002) on Subaru on June 6, 2002. We used one multi-slit mask containing slits for 4 LBG candidates. We also observed 5 objects selected by other criteria including Lyman α emitter (LAE) candidates at z=4.9

¹¹ Part of the GTO data are now included in the data of the SDF key project; e.g., about one-third of the i' and z' data presented in Kodaira et al. (2003) were taken in the GTOs.

¹² In Figure 2, the region in the lower right corner surrounded by the dashed line and the solid line corresponds to the position of the w93c2. In Figure 3, the upper right corner, where no data exist, corresponds to the position of the w93c2.

¹³ In Figure 2, the region in the lower left corner corresponds to the position of the w67c1.

(SDS IV). Thus, the number of galaxies for which we took spectra is 4+5=9. We chose the 300 line mm⁻¹ grating with a dispersion of 1.4 Å pixel⁻¹ and a wavelength coverage of 4700-9400Å. The sensitivity decreases in blue wavelengths ($\lesssim 6000$ Å; see Kashikawa et al. 2002). We adopted a slit width of 0".8, which gave a spectral resolution of 9.8Å. We made 2 hr exposure for each object. The seeing size of the night was 0".7–0".8. The continuum flux limit of our spectra was 6.3×10^{-19} erg s⁻¹ cm⁻² Å⁻¹ with the 5σ significance level. In addition to these nine spectra, we use 76 spectra given by SDS III which were taken during the guaranteed time observations of FOCAS in 2001. The details of the spectra are described in section 3.1.

2.2. Data Reduction

We develop the pipeline software, SDFRED, (Ouchi et al. 2003b) to reduce Suprime-Cam data. The core programs of SDFRED are taken from IRAF, SExtractor (Bertin & Arnouts 1996), and the mosaic-CCD data reduction software (Yagi et al. 2002). SDFRED includes a set of optimized parameters which are common to any Suprime-Cam data, and it accepts free parameters dependent on conditions of data. This pipeline software is open to the public, and a manual of the software and instructions for installation are given in Ouchi et al. (2003b). We reduce all the observed data of good quality with SDFRED, and make stacked images for all bandpasses. We align these stacked images using hundreds of stellar objects in each image. Then, we smooth the images with Gaussian kernels to match their seeing sizes. The final images have a PSF FWHM of 0".9 (SDF) and 0."98 (SXDF).

2.2.1. Photometric Zero-Points

We calculate photometric zero-points from photometry of standard stars with a $10''\phi$ aperture (Hereafter ϕ indicates the diameter of a circular aperture). We use the zero-points obtained in photometric nights with airmass correction (Ouchi et al. 2001). We check these photometric zero points using colors of 175 Galactic stars calculated from spectra given in Gunn & Stryker (1983). Since the FoV of Suprime-Cam is large enough to detect more than 100 bright stars with $i' \lesssim 23$, we can examine the photometric zero-points using various two-color diagrams. We find that the colors of stellar objects in our data are consistent with those of Gunn & Stryker's stars, except for some two-color diagrams in which an offset of $\simeq 0.05$ mag is seen. Such offsets are probably due to photometric errors of standard stars observed in slightly non-photometric conditions. We correct the zero points by about $\simeq 0.05$ mag, so that the observed colors of stellar objects match the synthetic colors of Gunn & Stryker's stars. The photometriczero points thus obtained are regarded as more accurate than 0.05 mag.

2.2.2. Photometric Catalogs

Source detection and photometry are performed using SExtractor version 2.1.6 (Bertin & Arnouts 1996). We measure both MAG_AUTO of SExtractor and $2''\phi$ aperture magnitudes; a $2''\phi$ aperture diameter is twice as large as the seeing size, i.e., 1''.8 and 2''.0 for the SDF and SXDF data, respectively. In order to obtain faint PSF-like objects with a good signal-to-noise ratio, we do not adopt

MAG_AUTO as total magnitudes. Instead, we use for total magnitudes $2''\phi$ aperture magnitudes after applying an aperture correction of 0.2 magnitude. We present in section 3.1 the difference between MAG_AUTO and $2''\phi$ aperture magnitudes after aperture correction. We make i'and z'-detection catalogs for both the SDF and the SXDF data. We limit the catalogs to i' < 26.5 and z' < 26.0(i' < 26.0 and z' < 25.5) for the i'- and z'-detection catalogs of the SDF (SXDF), in order to provide a reasonable level of photometric completeness. These limiting magnitudes are defined for a 2'' diameter aperture. Our i'detection and z'-detection catalogs contain 45,923 (39,301) and 37,486 (34,024) objects for the SDF (SXDF), respectively. We correct the magnitudes of objects for Galactic extinction, E(B - V) = 0.019 and E(B - V) = 0.020(Schlegel, Finkbeiner, & Davis 1998) for the SDF and SXDF, respectively.

We measure 3σ limiting magnitudes of the images, which are defined as the 3σ levels of sky noise on a $2''\phi$ diameter. For each image, we measure sky counts in a number of 2''-diameter circular apertures which are located at randomly selected positions in the image. Then, we draw a histogram of the sky counts, and fit a Gaussian function to the histogram to obtain a 1σ noise. When we fit a Gaussian function, we omit the positive tail of the histogram which is affected by objects. The limiting magnitudes are presented in Table 1. Note that we did not simply calculate the 3σ limiting magnitudes by scaling a 1σ noise in one pixel to a 2'' diameter area. Since this simple scaling results in a very optimistic limiting magnitude as discussed in Furusawa (2002) and Labbé et al. (2003), we use the real noise values measured in $2''\phi$ apertures.

2.2.3. Astrometry

Since we correct geometric distortion of images through the data reduction, relative astrometry is good enough for this work. Relative error is less than 1 pixel (0''.202/pixel). However, we need to obtain absolute astrometry for followup spectroscopy. We calibrate coordinates of objects using faint objects (B = 19 - 20) given in USNO A2.0 catalog (Monet et al. 1998). Although positional accuracies of USNO objects are not so good (typically 0."25), there are no other calibrators which are faint enough (so that they are not saturated in our images). We use 136 (97) USNO objects which are not saturated in the B-band image in the SDF (SXDF). They are uniformly distributed over the images. We obtain the absolute coordinates of our objects with these USNO objects. The errors in the absolute positions of objects in (α, δ) are estimated to be less than 0.3 - 0.4 arcsec both in the SDF and in the SXDF.

3. PHOTOMETRIC SAMPLES OF LYMAN BREAK GALAXIES ${\rm AT}\ z = 3.5 - 5.2$

3.1. Definitions of BRi-, Viz-, and Riz-Lyman Break Galaxies

We make three photometric samples of LBGs by the following two-color selections. The first sample is for LBGs at $z \simeq 4$ selected by B-R vs. R-i'. They are referred to as BRi-LBGs. BRi-LBGs are galaxies whose Lyman break enters into the B band and whose flat UV continuum is sampled in the R and i' bands, and these galaxies

are identified by their red B-R and blue R-i' colors. Similarly, the second is for LBGs at $z\simeq 5$ selected by V-i' and i'-z', and we refer to them as Viz-LBGs. The third is for LBGs at $z\simeq 5$ selected by R-i' and i'-z', and we refer to them as Riz-LBGs.

For $z\gtrsim 4$ objects, the UV continuum shortward of 1216Å is damped by the Ly α absorption of the intergalactic medium (IGM). Since the depression at 1216Å is as strong as that at 912Å (Lyman break) for galaxies at $z\gtrsim 4$, LBGs identified by the above two-color selections are not "Lyman break" galaxies but "Lyman break + Ly α absorption" galaxies in reality. The central redshift of these samples is shifted toward lower redshifts than the one calculated by dividing the central wavelength of the bluest band by 912Å. For example, Riz-LBGs are expected to be located around at $z\sim 6500/912-1=6.1$, but the actual redshifts are $z\sim 5$ (section 3.2).

Figures 4-6 illustrate how to isolate LBGs from foreground objects including Galactic stars. These figures indicate that LBGs can be isolated from low-z galaxies and Galactic stars by their red break colors (B-R,V-i'), and R-i') and their blue continuum colors (R-i',i'-z'), and i'-z'). In order to define the selection criteria for LBGs quantitatively, and estimate the sample completeness and contamination, we use 85 spectroscopically identified objects in our fields and 1048 galaxies in the photometric redshift catalog of HDF-N given by Furusawa et al. (2000) as explained in the following.

Our 85 spectroscopically identified objects come from two sources. One is the sample of 9 objects for which we carried out spectroscopic follow-up observations and the other is the spectroscopic catalog of 76 SDF objects compiled by SDS III. The nine spectra are (i) 4 LBG candidates whose colors are close to those of model galaxies at z > 3.5 (Figures 4-6) and (ii) 5 objects including LAE candidates of SDS II (see SDS IV). We identify that these 4 LBG candidates are real LBGs at z = 4.140, z = 4.250, z = 4.270, and z = 4.865 (These SDFJ132413.3+274207, SDFJ132416.3+274355, SDFJ132413.1+274116, and SDFJ132410.5+274254 in Figure 7). In the 76 spectra, there are two LBGs at $z>3.5\colon z=3.845$ and 4.600. ¹⁴ In summary, we have 85 (=9+76) spectroscopically identified objects at $0 \le z < 5$, and 6 among them are found to be LBGs at z > 3.5. Out of the rest (79 objects), three are LBGs at 3.0 < z < 3.5, four are LAEs at z = 4.9 which are only detected in a narrow-band image (SDS II), and the other 72 objects are either blue dwarf galaxies with emission lines, or red latetype galaxies up to at z = 1.1, or late-type Galactic stars. Figure 7 shows the spectra and snap shots of the identified 6 LBGs, and Table 2 summarizes their properties.

We compare colors of galaxies in our LBG samples with colors of the 85 spectroscopically identified objects. The 85 spectroscopically identified objects are plotted on the two-color diagrams in Figures 8-10; blue circles are for interlopers and red circles are for LBGs at 3.5 < z < 4.5, 4.2 < z < 5.2, and 4.6 < z < 5.2 for BRi-LBGs, Viz-LBGs, and Riz-LBGs, respectively. As expected, spectroscopically identified high-z galaxies are located in the

upper-left part of the two-color diagrams. We define the selection criteria for LBGs, so that the criteria select LBGs with a reasonably high completeness and with a low contamination from interlopers. Since the number of spectroscopically confirmed objects is very small (especially for high-z galaxies), we determine the selection criteria of LBGs by simulations.

We use the best-fit SEDs of objects in the HDF-N photometric redshift catalog given by Furusawa et al. (2000). The HDF-N catalog is an appropriate catalog to be compared with our data, since it contains a number of galaxies at z = 4 - 6 calibrated with spectroscopic identifications. Another advantage of the HDF-N catalog is that it has not only blue (in UV continuum) galaxies but also red (in UV continuum) galaxies which usually escape from Lyman break selection criteria. We already show in Figures 4-6 colors of the 1048 HDF-N galaxies which are calculated by convolving the best-fit SEDs with the response functions of the Suprime-Cam filters. Since the colors of these HDF-N galaxies are calculated from the best-fit SEDs, they are free from random photometric noise. The colors of objects in our catalogs, on the other hand, include random errors whose amplitudes are dependent on apparent magnitudes and local sky fluctuations. So as to evaluate these random errors, we generate artificial galaxies that mimic the HDF-N galaxies, and distribute them randomly on our original images after adding Poisson noise according to their original brightness. Then, we detect these simulated objects and measure their brightness in the same manner as for our photometric catalogs (section 2.2.2). We iterate this process 100 times and derive probability maps of the detected objects in two-color diagrams. We define low-z interlopers as galaxies whose redshifts are lower than z=3in the original photometric-redshift catalog. In Figures 8-10, we show the probability maps of the low-z interlopers, i.e., probability maps of contamination, thus obtained. To derive probability maps of high-z galaxies, we carry out additional simulations since the number of high-z galaxies in Furusawa et al.'s (2000) catalog is not large (52 galaxies at z > 4). Here, high-z galaxies are defined as galaxies whose redshifts are close to the expected central redshift given by the color selection for each of the three LBG samples. Assuming that the color distribution found for the high-z galaxies in the HDF-N catalog is universal and independent of i' (and z') magnitude, we make a mock catalog of 1648 galaxies at $z \geq 2.5$ whose i'- or z'-band magnitudes are scaled from 23.0 mag to 27.0 mag with a 0.5-magnitude interval. Then we distribute these galaxies on our original images and detect them in the same manner as for the estimation of low-z interlopers. We iterate this process 100 times, and we obtain probability maps of high-z galaxies. In Figures 8-10, we show the probability maps of high-z galaxies, i.e., probability maps of completeness. We also plot the spectroscopically identified objects in Figures 8-10. The probability maps are fairly well consistent with the color distributions of the spectroscopically identified objects.

Based on the probability maps of interlopers and high-z

 $^{^{14}}$ The original catalog of SDS III has four LBGs at z > 3.5. However, one galaxy at z = 4.620 has spectroscopic features similar to late-type stars. Furthermore, the magnitude of this object is bright, z' = 23.66, and its profile is stellar. Therefore, we regard this object as a Galactic star. Another LBG at z = 3.810 is blended in our image, and we cannot detect this LBG as a single object. Thus, we use the remaining two LBGs for our analysis.

galaxies, we determine the selection criteria of three LBG samples which yield small contaminants and keep completeness high enough as:

$$B-R > 1.2$$
, $R-i' < 0.7$, $B-R > 1.6(R-i') + 1.9$ ($BRi - LBGs$), (1) clear to us. The boundary of selection criteria of Iwata et $V-i' > 1.2$, $i'-z' < 0.7$, $V-i' > 1.8(i'-z') + 1.7$ ($Viz - LBGs$), (2) al. (2003) is very close to the colors of elliptical galaxies at $R-i' > 1.2$, $i'-z' < 0.7$, $R-i' > 1.0(i'-z') + 1.0$ ($Riz - LBGs$), (3) $Z = 0.5 - 1.0$; the separation between the boundary and

respectively. In Figures 8-10, green lines show these criteria. These criteria reject not only the sequences of low-zinterlopers, but also tails of low-z interlopers scattered by photometric errors. Since the number density of low-zinterlopers is quite large, those scattered by photometric errors become significant in number density. The upperleft panel of Figure 8 shows that the selection criteria of BRi-LBGs reject all the spectroscopically identified low-z objects, and that the criteria select all the spectroscopically identified high-z galaxies at z = 3.5 - 4.5. On the other hand, the upper-left panel of Figure 9 shows that the selection criteria of Viz-LBGs reject all the spectroscopically identified low-z objects, but that the criteria miss two spectroscopically identified high-z galaxies at z =4.2 - 5.2. These two galaxies are SDFJ132416.3+274355 and SDFJ132413.1+274116. Their redshifts, z = 4.250and 4.270 are close to the lowest redshift (z = 4.2) that satisfies the criteria. This result is consistent with our simulations which show that the criteria select just $\sim 20\%$ of $z \simeq 4.3$ galaxies (see Figure 12; details are discussed later in this section). In the upper-left panel of Figure 10, the criteria of Riz-LBGs reject all the spectroscopically identified low-z interlopers, but that the galaxy at z = 4.865is marginally missed. Similarly, our simulations show that the criteria select about half of the galaxies at z = 4.9 (see Figure 12). In summary, we can well estimate the completeness of high-z galaxies as a function of redshift from our simulations.

The right panel of Figure 9 shows that the Viz-LBG sample of the SXDF contains a large number of contaminants. This is because the signal-to-noise ratio of the SXDF V-band data is worse than that of the SDF V-band data. In order to select Viz-LBGs in the SXDF with a smaller number of contaminants, we define the Viz-LBG selection for the SXDF data as

$$V - i' > 1.2, i' - z' < 0.7, V - i' > 1.8(i' - z') + 2.3.$$
 (4)

Since these criteria are quite tight, the completeness of the Viz-LBG sample is very low (see Figure 12).

We apply these selection criteria to our photometric catalogs. We use i'-detection catalogs for BRi-LBGs, and z'detection catalogs for Viz-LBGs and Riz-LBGs. We find 1,438 (732), 246(34), and 68 (38) objects for BRi-LBGs, Viz-LBGs, and Riz-LBGs in the SDF (SXDF). Thus we obtain LBG samples composed of 2,556 ($\simeq 2,600$) LBGs in total, which are the largest LBG samples at z=4-5, to date. We refer to these LBG samples as the photometric samples of LBGs. Table 3 summarizes the photometric samples.

We show number counts of LBGs in our samples in Figure 11, together with those obtained by Steidel et al. (1999) and Iwata et al. (2003). We find that the number counts of our LBGs are fairly comparable to those of Steidel et al. (1999) who selected LBGs at $z=4.1\pm0.5$ by a two-color diagram of Gn - R vs. R - I. On the other hand, there is a large discrepancy between our counts (at

bright magnitudes) and those by Iwata et al. (2003) who selected LBGs at $z = 5.0 \pm 0.5$ by a two-color diagram of $V - I_c$ vs. $I_c - z'$. The reason for this discrepancy is not clear to us. The boundary of selection criteria of Iwata et R - i' > 1.2, i' - z' < 0.7, R - i' > 1.0(i' - z') + 1.0 (Riz - LBGs),(3) $z \simeq 0.5 - 1.0$; the separation between the boundary and the colors of foreground galaxies is only about 0.05 magnitude in $I_c - z'$. In reality, the two-color diagram of Iwata et al. (2003) shows that their criteria select a number of objects from the outskirts of low-z objects' color sequence in the brightest magnitude range ($I_c < 23.5$; Figure 2 (d) of Iwata et al. 2003). On the other hand, our selection criteria have a margin between LBGs and foreground objects by at least 0.2 magnitude. Photometric errors and small offsets in photometric zero-points would easily introduce errors of 0.05 magnitude. Therefore, we infer that Iwata et al.'s LBG sample suffers from bright foreground galaxies, which strongly affect the bright end of number counts for LBGs.

3.2. Completeness and Contamination of the Samples

We use the results of the simulations described in section 3.1 in order to estimate the redshift distribution, completeness, and contamination of the LBG samples. Simulated galaxies are sorted into redshift and magnitude bins with bin sizes of $\Delta z = 0.2$ and $\Delta m = 0.5$, respectively. We count the number of output high-z galaxies, $N_{\text{highz}}^{out}(m, z)$, and the number of input high-z galaxies, $N_{\text{highz}}^{in}(m, z)$, in each of the redshift and magnitude bins. We define the completeness as a function of redshift for our LBG sample

$$C(m,z) = \frac{N_{\text{highz}}^{out}(m,z)}{N_{\text{highz}}^{in}(m,z)} \qquad (z \ge z_0),$$

$$C(m,z) = 0 \qquad (z < z_0),$$
(5)

where z_0 is the boundary redshift between low-z interlopers and LBGs. We adopt $z_0 = 3$ in our analysis. We plot C(m,z) of each LBG sample in Figure 12. The contamination of the sample is similarly defined as the ratio of the number of low-z $(z < z_0)$ interlopers to the number of all the objects satisfying the selection criteria. For contamination estimation, we use the total number of contaminants lying between z = 0 and $z = z_0$ in each magnitude bin, because we do not need the number of contaminants as a function of redshift. Figure 13 shows the total number of contaminants and the number of selected objects as a function of magnitude. We define the contamination for a given magnitude bin as

$$f_c(m) = \frac{\int_0^{z_0} AN_{\text{cont}}^{out}(m, z)dz}{N_{\text{all}}^{out}(m)},$$
 (6)

where $N_{\rm all}^{out}(m)$ and $N_{\rm cont}^{out}(m)$ are, respectively, the total number of selected objects and the number of selected interlopers in the magnitude bin, and A is a scaling factor to account for the difference in the area between HDF-N (i.e., 4 arcmin²) and the observed area (i.e., $\sim 600 \text{ arcmin}^2$).

3.3. Galaxies Escaping from our LBG Selections

We examine the fraction of high-z galaxies escaping from our LBG selections. There are two sources by which we miss to select high-z galaxies. One is the photometric errors, and the other is the sample bias due to the tight

selection criteria of LBGs which require the ideal features for identification, i.e., a clear Lyman break and flat-UV continuum. In the following sections, we investigate statistical features of our LBG sapmles. Since the photometric errors are random errors, correct statistical results are obtained using the contamination and completeness given in section 3.2. On the other hand, the sample bias systematically changes the statistical results, in spite of applying the corrections. Thus it is important to know how large fractions of high-z galaxies our LBG selections miss.

In order to investigate this sample bias, we use the HDF-N photo-z catalog by Furusawa et al. (2000) whose high-z galaxies are not biased as strongly as those selected from any LBG criteria which require a clear Lyman break and flat-UV continuum for identification. Since we need to know the systematic selection bias, we use the original colors of the photo-z catalog without photometric errors. Figure 14 plots the redshift distribution of the HDF-N photometric redshift galaxies. Galaxies which satisfy the selection criteria (eqs. (1)-(4)) are shown by filled histograms. The second, third, and bottom panels of Figure 14 present the redshift distribution of galaxies satisfying the BRi-LBG, Viz-LBG, and Riz-LBG selection criteria, respectively. These three panels show that most galaxies are selected if they are located at the central redshifts of the selection windows, $z \simeq 4.0$ for BRi-LBGs, $z \simeq 4.7$ for Viz-LBGs, $z \simeq 4.9$ for Riz-LBGs, while the selection completeness decreases toward the outskirts of the selection windows. These behaviors are reasonable, since galaxies are selected as LBGs if their Lyman breaks and/or Lyman α breaks enter in the bluest band, while Lyman α breaks do not enter the reddest band in each of the three band sets. The implicit assumption here is that high-zgalaxies are ideally characterized by their Lyman breaks and flat-UV continuum features. However, not all galaxies share such ideal features, and some galaxies may have weak Lyman break or steep (red) UV continuum. In order to estimate the fraction of galaxies escaping from our BRi-, Viz-, and Riz-LBG selections, we show the redshifts of all galaxies which are selected by at least one of eqs. (1), (2), and (3) in the top panel of Figure 14. If we focus on galaxies located at z = 3.9 - 5.1 (47 in total) where galaxies are well selected by the combination of BRi-, Viz-, and Riz-LBG selections, we find that 4 out of the 47 escape from the combination of these selections. The escaping galaxies are just $4/47 \simeq 10\%$ in number. We investigate differences between the four escaping galaxies and all the other galaxies using best-fit SEDs, which reflect stellar population (age and metallicity) and dust extinction (E(B-V)). We find no significant difference but for the amplitude of dust extinction. Figure 15 shows the histogram of E(B-V) of galaxies in the HDF-N photo-z catalog. It is found that galaxies with heavy dust extinction, $E(B-V) \gtrsim 0.4$, tend to be missed. This trend is reasonable because galaxies with heavy dust extinction are red in any colors and these galaxies with red colors are outside the LBG selection criteria.

On the other hand, Pascarelle, Windhorst, & Keel (1998) point out that about 50 % of galaxies escape from their LBG selection. Their claim, however, does not conflict with ours, since their definition of escaping galaxies is different from ours. Their claim is based on a compar-

is on between $z\simeq 4$ photo-z selected galaxies and galaxies selected by a LBG selection based on only one two-color diagram of B-V vs. V-I. If we calculate the completeness of our BRi-LBG sample following their definition, we find the completeness to be 61% (36 out of 59 galaxies at z=3.5-4.7), which is consistent with their value (50%). Dickinson (2000) has investigated the completeness of LBG selection with a similar definition to ours. He has compared the rest-frame UV selected LBGs with rest-frame optical selected photo-z galaxies, and found that 80% of the photo-z galaxies satisfy at least one of his LBG selections. Thus his results are consistent with ours.

According to the results shown above, we regard our LBG samples as 'extinction-uncorrected' rest-frame UV magnitude-limited samples, missing only $\sim 10\%$ of all galaxies (in number) brighter than given extinctionuncorrected UV magnitudes. Note that this very low missing fraction does not rule out the existence of a large population of very red galaxies whose extinction-uncorrected rest-frame UV magnitudes are much fainter than the limiting magnitudes of our samples because of heavy dust extinction. Similarly, our result is compatible with the existence of passive galaxies whose UV magnitudes are fainter than our limiting magnitudes. Indeed, recent deep nearinfrared observations have revealed a substantial number of red high-z galaxies which cannot be detected by the Lyman-break technique due to too faint optical magnitudes (Franx et al. 2003).

4. LUMINOSITY FUNCTIONS

4.1. Luminosity Functions of Lyman Break Galaxies

We derive luminosity functions (LFs) of LBGs at z=4-5 from our large samples; BRi-LBG, Viz-LBG, and Riz-LBG samples in the SDF and SXDF. Since we do not have redshifts for individual LBGs but only have the redshift distribution functions (i.e., probability density functions) given in Figure 12, we cannot calculate LFs by conventional methods (e.g., V/V_{max} method). However, our LBG samples are close to volume-limited samples, since for each sample the width of the redshift distribution divided by the mean redshift of the sample is sufficiently small. Hence, to calculate the LF for a given sample, we assign the mean redshift of the sample to all galaxies in it. For each sample, using the ratio of contamination (eq.6), we calculate the number density, n(m), of LBGs in a given magnitude bin by

$$n(m) = \frac{N(m)(1 - f_c(m))}{\int_{z_0}^{\infty} \frac{dV}{dz} C(m, z) dz},$$
 (7)

where N(m) is the number of objects satisfying the criteria in a given magnitude bin, $\frac{dV}{dz}$ is the differential volume, and $z_0(=3)$ is the boundary redshift between low-z interlopers and LBGs. Figure 16 plots the LFs of LBGs at $z=4.0\pm0.5~(BRi\text{-LBGs}),~z=4.7\pm0.5~(Viz\text{-LBGs}),$ and $z=4.9\pm0.3~(Riz\text{-LBGs}),$ where the abscissa is the absolute magnitude at the rest-frame 1700Å. The absolute magnitude at 1700Å is estimated from the i' magnitude for BRi-LBGs, and from the z' magnitude for Viz-LBGs and Riz-LBGs as follows. Most of the LBGs have PSF-like (FWHM $\simeq 1''$) shapes. We find from simulations made in section 3.1 that 2'' aperture magnitudes of PSF objects are fainter than the total magnitudes by

0.2 mag for FWHM $\simeq 1''$ on average. Thus, we calculate the total magnitude from the $2''\phi$ aperture magnitude, adding an aperture correction of -0.2 magnitude. Then, we add a constant k-correction factor, -0.03 for BRi-LBGs and -0.01 for Viz-LBGs and Riz-LBGs to the total magnitude. These values correspond to the median colors of $m_{1700}(z=4.0)-i'$, $m_{1700}(z=4.7)-z'$, and $m_{1700}(z=4.9)-z'$, respectively, for the HDF-N photo-z galaxies at z=3.5-4.5, z=4.2-5.2, and z=4.6-5.2 (Furusawa et al. 2000), where $m_{1700}(z=4.0)$, $m_{1700}(z=4.7)$, and $m_{1700}(z=4.9)$ are the magnitudes at the rest-frame 1700Å for galaxies at z=4.0, 4.7 and 4.9, respectively.

We find in Figure 16 that the LFs obtained from the SDF and the SXDF data show an excellent consistency. Thus we regard that our results do not suffer from field variance. Then we fit the Schecher function (Schechter 1976)

$$\psi(M)dM = C\phi^* \exp\left\{-C(\alpha+1)(M-M^*) - \exp[-C(M-M^*)]\right\} dM,$$
(8)

to the LFs, where $C \equiv 0.4 \ln(10)$, α is the power-law slope, ϕ^* is the normalization factor which has a dimension of the number density of galaxies, L^* is the characteristic luminosity, and M^* is the characteristic absolute magnitude. First, we fit the Schechter function with three free parameters, ϕ^* , M^* , and α , to the data, and find that these parameters cannot be constrained well except for the BRi-LBGs. Thus, for the Viz-LBG LF, we fix α and determine ϕ^* and M^* from fitting. For the Riz-LBG LF, we fix M^* as well as α , since even two-parameter fitting (ϕ^* and M^*) fails to give a reliable result. We adopt two values of α , -2.2 and -1.6, for the Viz-LBGs and Riz-LBGs, where $\alpha = -2.2$ is the best-fit value for our *BRi*-LBGs and $\alpha = -1.6$ is the best-fit value for z = 3 LBGs obtained by Steidel et al. (1999). By taking a common α value, we can make a fair comparison of the luminosity density extrapolated beyond the detection limits between our samples (see section 6). For the M^* of the Riz-LBG LF, we adopt an absolute magnitude calculated by linearly extrapolating the M^* values at z = 4.0 (BRi-LBGs) and z = 4.7(Viz-LBGs) to z = 4.9. We present the best-fit parameters for the three samples in Table 4, together with, for comparison, those for LAEs at z = 4.86 obtained by SDS II. Since the Schechter fit for Riz-LBGs is quite uncertain, we refer to the results of BRi-LBGs and Viz-LBGs as the Schechter parameters of z = 4 and z = 5 LBGs, respectively, in the following discussion (section 6), when we do not specify the sample names.

We plot the best-fit Schechter functions in Figure 16, together with those of LBGs at z=3 and 4 measured by Steidel et al. (1999), and UV-selected galaxies at $z\simeq 0$ given by Sullivan et al. (2000). Figure 16 shows that the LF at z=4 is not much different from that at z=3. However, the number density of galaxies at faint magnitudes appears to be slightly higher at z=4 than at z=3, resulting in the steeper faint-end slope, $\alpha=-2.2\pm0.2$, for our z=4 LBGs than $\alpha=-1.6$ obtained by Steidel et al. (1999) for z=3 LBGs. Hence, the slope of the LF may be steeper at z=4 than at z=3. Note that α for our LBGs is obtained from the BRi-LBG sample whose limiting magnitude reaches just M^*+1 . Thus the estimated slope of $\alpha=-2.2\pm0.2$ may include a large systematic error.

In Figure 16, we find that the number density of bright LBGs with $M_{1700} \sim -22$ decreases from z = 4 to z = 5. This tendency is found between BRi-LBGs and Riz-LBGs as well as BRi-LBGs and Viz-LBGs. Furthermore, the bright Riz-LBGs (i.e., LBGs at $z=4.9\pm0.3$) might be less numerous than the bright Viz-LBGs (i.e., LBGs at $z = 4.7 \pm 0.5$), implying that the number density of bright LBGs tends to drop at higher redshift, although the data points of Riz-LBGs have a large uncertainty. The difference between z = 4 and 5 is about one order in number density at $M_{1700} \sim -22$. Since the luminosity at 1700Å is approximately proportional to the star-formation rate (SFR), the observed decrease in bright LBGs with $M_{1700} \sim -22$ probably indicates that galaxies with high star-formation activity (SFR ~ 100 and $30h_{70}^{-2}M_{\odot}\text{yr}^{-1}$ for with and without extinction correction: details are described in section 7) are rarer at z = 5.

The error bars of the LFs in Figure 16 correspond to Poisson errors, and we have not included errors arising from the contamination and completeness corrections. In order to evaluate how these corrections affect the results, we vary the color-selection criteria (eqs. 1-4) by ± 0.15 magnitudes in each color (For example, we select BRi-LBGs with $B - R > 1.2 \pm 0.15$, $R - i' < 0.7 \pm 0.15$, $B-R > 1.6(R-i') + 1.9 \pm 0.15$). We derive number counts of the selected objects and correction factors (i.e., contamination and completeness) with the varied color-selection criteria. Then LFs are calculated from the number counts and the correction factors. We find that the LFs with the different criteria are consistent with the LFs plotted in Figure 16 within a factor \lesssim 2 in number density, and that the changes in criteria, although they give different correction factors, do not change the three tendencies, i.e., no significant change from z=3 to z=4, the decrease in number density at the bright magnitudes from z=4and z = 5, and the steep faint-end slope for z = 4 LBGs. Therefore, we conclude that these tendencies are real.

5. Dust extinction

5.1. UV Slopes versus E(B-V)

Steepness of the ultraviolet spectral slope (UV slope) of galaxies is a good measure of dust extinction, E(B-V), since the UV continuum is sensitive to dust extinction. Meurer, Heckman, & Calzetti (1999) show that the UV slope of local star-forming galaxies has a good correlation with infrared luminosity and dust extinction obtained from Balmer decrement (see Calzetti 2001 for a general review). The UV slope, β , is defined as

$$f_{\lambda} \propto \lambda^{\beta},$$
 (9)

where f_{λ} is the spectrum of a galaxy over the the rest-frame wavelength of $\sim 1000\text{Å}$ to $\sim 3000\text{Å}$ and β is the best-fit power-low index to the spectrum.

We estimate the dust extinction for our LBGs from the UV slope. We choose i'-z' color for estimating UV slopes of BRi-LBGs (at $z\simeq 4$), since R-i' and R-z' colors are affected by Lyman α emission and the trough of Lyman α absorption systems while i'-z' samples the continuum at $> 1216\text{\AA}$. We do not calculate UV slopes for Viz- or Riz-LBGs since Lyman α emission and the trough of Lyman α absorption systems enter the i' band. The UV slope, β , is originally defined as the index of the best-fit power-law

(eq. 9) in the wavelength range of $\sim 1000\text{Å}$ to $\sim 3000\text{Å}$, The definition of the wavelength range, however, varies among authors, e.g., 1100-3000Å and 1200-1800Å etc. (see Calzetti 2001). In order to measure the UV slope of LBGs at z=4 from the i'-z' color, we define β_{iz} as

$$\beta_{iz} \equiv -\frac{i' - z'}{2.5 \log(\frac{\lambda_c(i')}{\lambda_c(z')})}$$
$$= 5.42(i' - z'), \tag{10}$$

where $\lambda_c(i')$ and $\lambda_c(z')$ are the central wavelengths of the i' and z' bands.

We use the latest version of Bruzual & Charlot (1993) stellar population synthesis model (GISSEL00; Bruzual & Charlot 2003) convolved with the extinction curve of Calzetti et al. (2000). ¹⁵ We generate a template spectrum whose model parameters have the average values observed for LBGs at z=3, which are given in Papovich, Dickinson, & Ferguson (2001), that is, 70 Myr age, $0.2Z_{\odot}$ metallicity, and Salpeter IMF. Figure 17 compares the extinction- β relation of the template spectrum with the measurements for 43 nearby galaxies (Meurer, Heckman, & Calzetti 1999). The fitting is made over 1250-2600Å for both the template spectrum and for the nearby galaxies.

The extinction- β relation from our template spectrum (solid line) shows fairly good agreement with the data points of the nearby galaxies (filled circles), and with the best-fit line (dashed line) derived by Meurer, Heckman, & Calzetti (1999). The template, the typical LBG spectrum convolved with the dust extinction curve, is found to reproduce the empirical relation of nearby starburst galaxies. For the readers' eye guide, two different models are also plotted in Figure 17; one has the same age as the template model (70Myr) but a higher metallicity of $1Z_{\odot}$, and the other has the same metallicity as the template model $(0.2Z_{\odot})$ but a younger age of 90 Myr.

Then, we calculate the $E(B-V) - \beta_{iz}$ relation using the template model. The solid line of Figure 18 shows the relation for LBGs at z=4, which is expressed by a linear function:

$$E(B - V) = a + b\beta_{iz},\tag{11}$$

where a = 0.0162 and b = 0.218. Here i' and z'-band magnitudes correspond to average fluxes in the rest frame of 1500 ± 150 Å and 1800 ± 130 Å for LBGs at z=4. Note that i' and z'-band magnitudes measure the rest-frame fluxes of $1700 \pm 170 \text{Å}$ and $2000 \pm 140 \text{Å}$ for LBGs at z = 3.5, and $1400 \pm 140 \text{Å}$ and $1600 \pm 110 \text{Å}$ for LBGs at z = 4.5. Since β_{iz} is defined in the observed frame, this relation depends on the redshift of galaxies. We calculate β_{iz} for the template model at z = 3.5, 4.5, 4.7, and 5.2, where we apply the absorption of the Lyman α forest (Madau 1995) for the continuum flux at < 1216Å. Figure 18 displays the redshift dependence, showing that the dependence is only ± 0.05 in E(B-V) for galaxies with $E(B-V) \lesssim 0.5$ at z = 3.5 - 4.5, but that it exceeds $\Delta E(B - V) \simeq 0.1$ for galaxies at $z \gtrsim 4.7$. This large dependence for high-z galaxies is caused by Lyman α absorptions in the IGM; the Lyman α forest starts entering in the blue wavelength of the i'-band response function for objects at $z\gtrsim 4.7$, resulting in a systematic reddening in i'-z' color (hence, a systematic increase in β_{iz}). At z=3.5-4.5, the β_{iz} estimation is not affected either by the Lyman α emission line at 1216Å, or by the continuum emission from an older stellar population (e.g., F stars) at $\gtrsim 2700$ Å. Therefore, eq. (11) holds for LBGs at z=3.5-4.5 with an accuracy of 0.05 mag in E(B-V), but the equation does not work for LBGs at $z\gtrsim 4.7$. This is the reason why we estimate E(B-V) for BRi-LBGs at z=3.5-4.5 alone.

5.2. Dust Extinction of Lyman Break Galaxies at z=4

We calculate the extinction of our LBGs with eqs. (10) and (11). ¹⁶ We show the histogram of estimated E(B-V)in Figure 19. Because our Lyman-break selections identify galaxies with $E(B-V) \lesssim 0.5$ as shown in Figure 15, we think that the estimated E(B-V) values larger than 0.5 are spurious. In Figure 19, we limit our sample to 651 LBGs brighter than i' = 25.5 for the SDF and i' = 25.0 for the SXDF. This is because we need to measure colors up to $i'-z' \simeq 0.5$, which corresponds to $E(B-V) \simeq 0.5$, and the sample galaxies should have i' magnitudes brighter by 0.5 mag than the limiting magnitude of the z'-band image $(z'_{\text{lim}} = 26.0 \text{ for the SDF and } z'_{\text{lim}} = 25.5 \text{ for the SXDF}).$ However, there are still systematic biases in i' - z' in our LBG sample. One is that the LBG criteria select bluer galaxies more preferably at fainter magnitudes, since the LBG selection needs a red B-R color for the identification. This effect is also seen in the results of simulations as the difference in the red and yellow contours of the top panels in Figure 8. The other effect is that the edge of the BRi-LBG criteria at 1.2 < B - R < 3.0 tends to reject red LBGs at redshift lower than $z \simeq 4$. So as to correct these biases, we carry out Monte Carlo simulations similar to those described in section 3.2. We use the template model of LBGs at z = 4 to calculate B - R and R - i'colors by varying extinction over 0.0 < E(B - V) < 1.0. We then make artificial galaxies which mimic the colors of the templates, and distribute them in the original images. We detect the artificial galaxies, and select them with the BRi-LBG criteria, and derive completeness as a function of E(B-V) for four i' magnitude bins. The results are plotted in the top panel of Figure 19. Using these completeness functions, we derive completeness-corrected distributions of E(B-V), which are shown by shaded histograms in Figure 19.

The mean values of E(B-V) calculated from the completeness-corrected histograms are 0.18, 0.13, 0.15, and 0.14 for magnitude bins of i'=23.5-24.0, 24.0-24.5, 24.5-25.0, and 25.0-25.5, respectively (Figure 19). The mean extinction of all the BRi-LBGs with i'<25.5 is $E(B-V)=0.15\pm0.03$. Thus the average extinction of LBGs at $z\simeq 4$ is estimated with the Calzetti's law to be about a factor of 4 for luminosity in 1700Å. Since i'=25.5 corresponds to $M_{1700}=-20.8$ whose magnitude is comparable to $M_{1700}^*=-21.0--20.6$ (Table 4), the mean extinction of $E(B-V)=0.15\pm0.03$ is for LBGs with $M\lesssim M^*$. No significant dependence of E(B-V) on the magnitude is found over 23.5< i'<25.5 (corresponding

¹⁵ Note that the Calzetti's attenuation curve provides the relation of $A(1600) = k_{1600}E(B-V)$, and $A(1700) = k_{1700}E(B-V)$, where $k_{1600} = 10$ and $k_{1700} = 9.6$.

¹⁶ Combination of equations (10) and (11) gives a relation between E(B-V) and i'-z' of $E(B-V)\simeq 0.0162+1.18(i'-z')$.

to $-23 < M_{1700} < -21$). Note that these magnitudes are apparent (i.e., before extinction correction) magnitudes, and this result indicates that LBGs at z=4 have no significant correlation between E(B-V) and the apparent magnitude. Adelberger & Steidel (2000) have obtained a similar result for LBGs at z=3. It is, however, found that there is a correlation between dust extinction and (extinction-corrected) intrinsic luminosity for our LBGs. Figure 19 shows that for each magnitude bin, E(B-V) spans the range of $0 \lesssim E(B-V) \lesssim 0.5$, which is larger than the statistical errors. This means that intrinsically brighter LBGs are generally more heavily attenuated by dust. The same tendency is found in LBGs at z=3 by Meurer, Heckman, & Calzetti (1999); Shapley et al. (2001).

5.3. Evolution of Dust Extinction at $0 \lesssim z \lesssim 4$

We investigate the evolution of dust extinction. Figure 20 shows the histogram of E(B-V) for the whole LBGs at z=4 (i'<25.5, i.e., $M \lesssim M^*$), together with those for local starburst galaxies (local SBs; Meurer, Heckman, & Calzetti 1999) and LBGs at z=3 (Adelberger & Steidel 2000; $R \leq 25.5$, i.e., $M \lesssim M^*+1$). The E(B-V) values for local galaxies and z=3 LBGs have also been derived from UV slopes using the extinction- β relation of Meurer, Heckman, & Calzetti (1999) and the dust extinction curve of Calzetti et al. (2000). The extinction- β relation used in these papers is similar to ours which is shown in Figure 17 with only a small difference of $\Delta A_{1600} \lesssim 0.3$ corresponding to $\Delta E(B-V) \lesssim 0.03$.

The mean dust extinction is 0.20, 0.15, and 0.15 for local SBs, z = 3 LBGs, and z = 4 LBGs, respectively. If taken at face value, the mean dust extinction of LBGs at z = 3 - 4 is lower than that of local starburst galaxies. However, this trend may be superficial. The sample of local starbursts is based on a combination of galaxy catalogs which are constructed by observations at various wavelengths, while the LBG samples are UV-continuum limited samples (section 3.3). One cannot rule out the possibility that the observed trend of E(B-V) is due to the selection effect that UV-continuum limited samples are likely to be biased toward dust-poor objects. On the other hand, the sample selections of LBGs at z=3 and z = 4 are quite similar. The very small difference in the mean extinction between z = 3 and z = 4 LBGs, at most $\Delta E(B-V) < 0.03$, indicates that there is no evolution in dust extinction between z = 3 and 4.

6. EVOLUTION OF UV-LUMINOSITY DENSITY

We calculate UV-luminosity densities of our LBGs from the luminosity functions (LFs) derived in section 4. First, we integrate the LFs (Figure 16) down to the magnitudes of the faintest LBGs in our samples (i.e., down to $M_{1700} = -19.8, -20.5, -20.5$ for BRi-LBGs, Viz-LBGs, and Riz-LBGs, respectively) to obtain observed UV-luminosity densities, $\rho_{\text{UV}}^{\text{obs}}$, the lower limits of the UV-luminosity density. The total UV-luminosity density has to be larger than $\rho_{\text{UV}}^{\text{obs}}$ by the contribution from galaxies fainter than the limiting magnitudes. In order to estimate the total UV-luminosity density, $\rho_{\text{UV}}^{\text{total}}$, we extrapolate the

LFs down to $L=0.1L^*$. We also calculate the total UV-luminosity density by extrapolating the LFs down to L=0 assuming $\alpha=-1.6$ which are the upper limits of the UV-luminosity density. To derive $\rho_{\rm UV}^{\rm total}$ down to L=0, we use the analytic formula $\rho_{\rm UV}^{\rm total}=L^*\phi^*\Gamma(\alpha+2)$. Both $\rho_{\rm UV}^{\rm obs}$ and $\rho_{\rm UV}^{\rm total}$ for BRi-LBGs, Viz-LBGs, and Riz-LBGs are summarized in Table 4. The upper limits of the UV-luminosity densities are shown in parentheses in Table 4. In Table 4, we also show the results of Lyman α emitters at $z=4.86\pm0.03$ which are similarly calculated from the best-fit UV-luminosity function obtained in SDS II.

We discuss the evolution of star-formation rate (section 6.1) and the reionization of the universe (section 6.2) using the $\rho_{\rm UV}^{\rm total}$ estimates. We do not use $\rho_{\rm UV}^{\rm obs}$ for our discussion, since our data are still considerably shallow and thus objects fainter than the limiting magnitudes will certainly dominate the total luminosity density. The $\rho_{\text{UV}}^{\text{total}}$ values for $\alpha = -2.2$ and -1.6 gives an estimate of how much the $\rho_{\rm UV}^{\rm total}$ values are dependent on the choice of the faint-end slope. We find in Table 4 that for each sample, the $\rho_{\text{IIV}}^{\text{total}}$ values down to $L = 0.1L^*$ for the two α agree with each other within the errors. Furthermore, the trend that $\rho_{\text{HV}}^{\text{total}}$ decreases slightly from z=4 to 5 is consistently seen for both α values. Thus, the error in $\rho_{\rm UV}^{\rm total}$ due to the change in α seems to be modest over a reasonable range of α . Although the choise of the faint-end slope does not affect much on the results, the estimated total luminosity density is based on the large extrapolation to the observed luminosity density. We show how much this extrapolation affects to the results of the following section (section 6.1.1). Since we obtain the upper limits of luminosity densities for the case of $\alpha = -1.6$, we adopt the luminosity densities from the Schechter parameters with $\alpha = -1.6$ (fixed) for the following sections.

6.1. Star-Formation Rate Density

6.1.1. Evolution of Star-formation Rate Density Based on L_{2000}

We calculate the cosmic star-formation rate (SFR) from the UV-luminosity density, $\rho_{\rm UV}^{\rm total}$. We use the relation between the UV luminosity and the star formation rate given by Madau, Pozzetti, & Dickinson (1998):

$$SFR(M_{\odot}yr^{-1}) = L_{UV}(erg s^{-1}Hz^{-1})/(8 \times 10^{27}), \quad (12)$$

where $L_{\rm UV}$ is the UV luminosity measured in $1500\text{\AA}-2800\text{Å}$. ¹⁷ This relation assumes that galaxies have the Salpeter IMF with solar metallicity. This conversion is insensitive to the difference in the star formation history especially for the far-UV luminosity at $\lesssim 2000\text{\AA}$, since UV fluxes are produced by massive OB stars whose lifetimes are $\lesssim 2 \times 10^7$ yr (Madau, Pozzetti, & Dickinson 1998). Figure 21 shows the cosmic SFRs of z=4-5 LBGs in our sample, together with those of galaxies at z=0 (Sullivan et al. 2000), z=0-1 (Cowie, Songaila, Hu, & Cohen 1996), and z=3-4 (Steidel et al. 1999). These cosmic SFRs (and UV-luminosity densities) have been corrected for the same amount of dust correction, E(B-V)=0.15, since there is no significant change in the observed E(B-V) value over z=0-4.5 (section 5.3).

 $^{^{17}}$ The conversion factor in eq. (12) is 8.0×10^{27} for the luminosity at 1500Å and 7.9×10^{27} for the luminosity at 2800Å (Madau, Pozzetti, & Dickinson 1998).

We also show the cosmic SFRs at $z=0,\,0.2,\,0.9,\,$ and 1.3 estimated from H α luminosity density given by Gallego, Zamorano, Aragon-Salamanca, & Rego (1995), Tresse & Maddox (1998), Glazebrook et al. (1999), and Yan et al. (1999), respectively. Note that the cosmic SFRs estimated from the UV-luminosity density with dust correction are comparable to those calculated from H α luminosity density. Figure 21 indicates that there is no significant change, or possibly a slight decline, in the cosmic SFR from $z\simeq 1$ up to $z\simeq 5$. The possible decline from z=4 to z=5 is due to the decrease in luminosity density found in the previous section.

In Figure 21, we also plot the star-formation rate calculated from $\rho_{\rm UV}^{\rm obs}$ (open circles). Since $\rho_{\rm UV}^{\rm obs}$ is the UV-luminosity density contributed by the bright portion of LFs for which data exist, these are robust lower limits of the star-formation rate. We find from our data at z=4that the cosmic SFR is almost constant from $z \simeq 1$ to z=4.5 even when we use $ho_{\mathrm{UV}}^{\mathrm{obs}}$ instead of $ho_{\mathrm{UV}}^{\mathrm{tot}}$. It should be noted that the lower limit at z = 4 obtained by Steidel et al. (1999) is much lower than ours based on $\rho_{\rm UV}^{\rm obs}$ due to their shallow data. Our data have improved largely the robust lower limit of the cosmic SFR at z = 4. On the other hand, the lower limit derived for our z = 5 LBGs is not high enough to reject a large decline of the cosmic SFR at z = 5. However the true cosmic SFR at z=5 is presumably high as the estimate from $\rho_{\rm UV}^{\rm tot}$ indicates, since we find at $z\lesssim 1$ a good agreement between the cosmic SFRs derived from total ${\rm H}\alpha$ luminosity densities and those based on UV-luminosity densities which are estimated from extrapolated LFs with dustextinction correction. We fit the cosmic SFR data including those based on $H\alpha$ luminosity density by the analytic function of redshift given in Cole et al. (2001): cosmic $SFR = (a+bz)/(1+(z/c)^d)h_{70}^{-2}M_{\odot}/\text{yr/Mpc}^3$, and obtain $a=0.0039,\ b=0.13,\ c=1.6,\ \text{and}\ d=1.8$. We show the best-fit function with errors by the shaded region in Figure 21.

6.1.2. Stellar Mass Assembly History

We estimate the stellar mass density accumulated from z=6, using the best-fit function of cosmic SFR obtained in section 6.1.1. We show the stellar mass density calculated by integrating the cosmic SFR over cosmic time as a function of redshift by the shaded region in the bottom panel of Figure 21, together with those measured directly from the stellar mass function of galaxies at z = 0-3 (Cole et al. 2001; Cohen 2002; Dickinson, Papovich, Ferguson, & Budavári 2003). Since the cosmic SFRs at high-z are calculated from an extrapolation of luminosity function, they may overestimate the real cosmic SFRs, if the true luminosity functions have flatter slopes. Thus, we also estimate the lower-limits of stellar mass density from the observed luminosity densities (open symbols in the top panel of Figure 21). The lower-limit values are connected by the dashed line in Figure 21.

At z = 0 - 1, the stellar mass densities derived directly from the stellar mass functions are consistent with those calculated from the cosmic SFRs (both the total densities, $\rho_{\rm UV}^{\rm total}$, and the lower limits, $\rho_{\rm UV}^{\rm obs}$) within the uncertainties.

At z = 1 - 3, however, the stellar mass densities based on the stellar mass functions are as low as the lower limits calculated from $\rho_{\rm UV}^{\rm obs}$ and about a factor of three lower than the total densities calculated from $\rho_{\text{IIV}}^{\text{total}}$. There are at least four possible reasons for this discrepancy. First, the stellar mass densities obtained by Dickinson, Papovich, Ferguson, & Budavári (2003) may suffer from a large cosmic variance because they are based on data of the HDF-N, a very small patch of the sky. Second, the stellar population synthesis models used to derive the cosmic SFRs and the stellar mass functions may not be appropriate for high-z galaxies. For example, both our analysis and Dickinson, Papovich, Ferguson, & Budavári (2003)'s adopt the Salpeter IMF. However, it is possible that high-z galaxies have a different IMF (e.g., top-heavy IMF). Third, Dickinson, Papovich, Ferguson, & Budavári (2003) assume a constant mass-to-luminosity ratio for faint galaxies whose stellar masses are not measured by fitting their stellar synthesis models. If, however, the actual mass-to-luminosity ratio increases with decreasing luminosity, the stellar mass densities obtained by Dickinson, Papovich, Ferguson, & Budavári (2003) are underestimates of the true values. Fourth, while we assume that the dust extinction of LBGs is constant with luminosity, LBGs fainter than the detection limits may have smaller extinction. Such a decrease in E(B-V) could change largely the total cosmic SFR, since the contribution to the cosmic SFR from LBGs fainter than the detection limits is significant.

6.2. Contribution to the Reionization of the Universe

The IGM has been ionized since, at least, z=6 (Becker et al. 2001; Fan et al. 2002). Since a large number of ionized hydrogens recombine in a relatively short time scale, ionizing photons have to be supplied by objects at each epoch to keep the IGM ionized. Madau, Haardt, & Rees (1999) give a formula to calculate the critical rate of ionizing photons, $\dot{N}_{\rm ion}^{\rm cr}$, required to maintain the ionization of IGM. The original formula is given in Einstein-de Sitter cosmology, and we rewrite their formula, which can be applied to our Λ -cosmology ($h=0.7, \Omega_m=0.3, \Omega_{\Lambda}=0.7$) with an acceptable accuracy at $3\lesssim z \lesssim 6$, as:

$$\dot{N}_{\rm ion}^{\rm cr} = (10^{51.0} \text{ s}^{-1} \text{Mpc}^{-3}) C_{30} \left(\frac{1+z}{6}\right)^3 \left(\frac{\Omega_m h^2}{0.02}\right)^2,$$
(13)

where C_{30} is the ionized hydrogen clumping factor normalized by 30. The fiducial value for this clumping factor is $C_{30} = 1$. The main uncertainty in this critical rate is originated from this clumping factor, which is estimated to be of order ± 0.2 in the log (Madau, Haardt, & Rees 1999). We plot the critical rate as a function of redshift in Figure 22, together with the emission rate of ionizing photons from QSOs shown in Madau, Haardt, & Rees (1999). Figure 22 indicates that the QSOs' production rate of ionizing photons, $N_{\rm ion}({\rm QSO})$, is less than the critical rate at $z \geq 3.6$.

 $z\gtrsim 3.6$. Since the number density of low-luminosity AGNs at high-z ($z\sim 3$) is much lower than that of LBGs at similar redshifts (3%; Steidel et al. 2002), the deficit of ionizing

¹⁸ The recombination time scale depends on the density of IGM and thus on redshift. The recombination time scale at z=3 is estimated to be ≈ 300 Myr (Madau, Haardt, & Rees 1999).

photons should be supplied from massive stars in galaxies. We estimate the emission rate of ionizing photons per unit volume from galaxies, $\dot{N}_{\rm ion}({\rm GAL})$, at z=4 and 5. The emission rate is related to the cosmic SFR, i.e., the star-formation rate density (SFRD):

$$\dot{N}_{\rm ion}({\rm GAL}) = C f_{\rm esc} {\rm SFRD}[{\rm M}_{\odot} {\rm yr}^{-1} {\rm Mpc}^{-3}] {\rm Numbers}^{-1} {\rm Mpc}^{-3},$$
(14)

where C is a conversion factor, $f_{\rm esc}$ is the escape fraction of ionizing photons, and SFRD is the star-formation rate of galaxies per unit volume (Madau, Haardt, & Rees 1999). Madau, Haardt, & Rees (1999) estimate $C = 10^{53.1}$. We use eq. (12) to calculate the star-formation rate.

Among the above parameters, the escape fraction of ionizing photons is unknown. Here we give an constraint on the escape fraction for LBGs at z=4 and z=5 using our data as follows. Since the IGM at $z\lesssim 6$ is ionized (Becker et al. 2001), the sum of ionizing photons from QSOs and galaxies should exceed the critical rate, at least, at $z\lesssim 6$:

$$\dot{N}_{\rm ion}^{\rm cr} < \dot{N}_{\rm ion}({\rm GAL}) + \dot{N}_{\rm ion}({\rm QSO}).$$
 (15)

First, we consider the escape fraction of our LBGs at z = 5. We estimate the critical rate using eq. (13) to be $\dot{N}_{\rm ion}^{\rm cr} = 8.8^{+5.1}_{-3.2} \times 10^{50}$, and we find $\dot{N}_{\rm ion}({\rm QSO}) = 3.0 \times 10^{50}$ (Madau, Haardt, & Rees 1999). On the other hand, the number density of ionizing photons from galaxies is calculated to be $\dot{N}_{\rm ion}({\rm GAL}) = 4.4 \pm 1.9 \times 10^{51} f_{\rm esc}$. Substituting these values for eq. (15), we find $f_{\rm esc} > 0.13^{+0.13}_{-0.09}$ for LBGs at z = 5. Similarly we obtain $f_{\rm esc} > 0.02^{+0.05}_{-0.02}$ for LBGs at z = 4. Note that the errors in $f_{\rm esc}$ include the uncertainty in $C_{\rm esc} + 0.2$ day. Thus, z = 1in C_{30} , ± 0.2 dex. Thus, we place a moderately significant constraint on the escape fraction for LBGs at z = 5, but not for LBGs at z = 4. Throughout the above discussion, we use the upper limits of the luminosity density (values in parentheses in Table 4) for LBGs at z = 4 and 5, which are obtained by integrating the LFs down to L=0. Since $f_{\rm esc}$ decreases with the luminosity density, the $f_{\rm esc}$ values calculated from these luminosity densities are regarded as conservative lower limits. We conclude that the escape fraction should be $f_{\rm esc}\gtrsim 0.13$ for LBGs at z=5. We plot in Figure 22 the sum of the number densities of ionizing photons from QSOs and galaxies at z = 3 - 5, assuming the lower-limit of the escape fraction to be $f_{\rm esc} = 0.13$.

7. DISCUSSION

7.1. Luminosity Functions and Dust Extinction of LBGs at z = 4-5

Luminosity functions (LFs) of LBGs show that the number of bright galaxies significantly decreases from z=4 to z=5, but little from z=3 to z=4. We find that the slope of the LF may steepen from z=3 to z=4. Our findings indicate that most of the bright $(M_{1700} \lesssim -22)$ galaxies appear between z=4 and 5, while faint $(M_{1700} \gtrsim -22)$ galaxies dominate in number density at $z \gtrsim 4$. We find in Figure 16 that while our LF at z=4 agrees well with that derived by Steidel et al. (1999), our LF at z=5 is different from that obtained by Iwata et al. (2003) who claim that the LF at z=5 is similar to that at z=3. Thus there is a discrepancy between our and their findings. We examine the cause of this discrepancy. First of all, the field variance may be large for such bright LBGs, since the number of detected bright LBGs is as small as ~ 20 . However,

we find an excellent consistency between the LFs derived from the SDF and the SXDF. Thus the field variance is probably not the main reason for this discrepancy. Second, it is possible that the selection criteria of Iwata et al. (2003) would take a large number of contaminants in their LBG sample as discussed in section 3.1, resulting in the larger number density of bright LBGs than by ours.

We estimate the star-formation rate of bright LBGs with $M_{1700} \lesssim -22$ with eq. (12 to be $SFR_{\rm raw} \gtrsim 30h_{70}^{-2}M_{\odot}{\rm yr}^{-1}$ (see the upper abscissa axis of Figure 16 for the correspondence between M_{1700} and $SFR_{\rm raw}$). Since the UV luminosity of these LBGs has dust extinction of $E(B-V) \simeq 0.15$, the extinction corrected SFR is about a factor of 4 larger than $SFR_{\rm raw}$ (section 5.2). Thus LBGs with $M_{1700} \lesssim -22$ have intrinsic SFR of $\gtrsim 100h_{70}^{-2}M_{\odot}{\rm yr}^{-1}$. The deficit of $M_{1700} \lesssim -22$ LBGs at z=5 indicates that the number density of galaxies with high-star formation rate of $\gtrsim 100h_{70}^{-2}M_{\odot}{\rm yr}^{-1}$ drops from z=4 to z=5.

Our LFs are derived for UV-luminosity or, equivalently, star-formation rate. In general, galaxies with larger sizes and higher star-formation efficiencies have higher starformation rates. Thus, our findings imply that large galaxies are formed by subsequent mergers of small galaxies and/or that star-formation efficiency increases from z=5to z = 3. The former interpretation supports the picture of hierarchical clustering (e.g., Baugh, Cole, Frenk, & Lacey 1998; Kauffmann, Colberg, Diaferio, & White 1999; Weinberg, Hernquist, & Katz 2002) in which galaxies experience a number of mergers. On the other hand, the latter interpretation is not consistent with predictions from numerical simulations of hierarchical clustering. Since the cooling efficiency increases with the density of gas in dark halos, hot gas cools more efficiently at higher redshifts, resulting in a higher star-formation efficiency at a higher redshift (Hernquist & Springel 2003), which is opposite to the observed evolution. Thus, a decrease in the number density of dark halos predicted by the former scenario should explain the observed evolution of the LF at bright magnitudes. We calculate the cumulative number density of massive dark halos down to $10^{12} M_{\odot}$, where LBGs with $M_{1700} \lesssim -20.5$ are expected to reside (see the companion paper, SDS VI), and find that the number density of these massive halos is 44% (at z = 4) and 16% (at z = 5) of that at z=3. This decrease is roughly consistent with the observed decrease of bright LBGs in the number density from z = 3 to z = 5.

The slope of the LF at z = 4 is estimated to be $\alpha = -2.2 \pm 0.2$. Since the faintest LBGs in our sample are as bright as $M^* + 1$, the estimated slope should have large systematic errors. If taken at face value, the faintend slope of the LF at z=4 is steeper than that at z=3 $(\alpha = -1.6; \text{ Steidel et al. 1999}). \text{ Yan, Windhorst, & Co-}$ hen (2003) report that the faint-end slope of the LF for LBGs at $z \simeq 6$ may be as steep as $\alpha \sim -2$ from their deep HST/ACS data. Thus, the slope of the LF for LBGs may steepen at $z \gtrsim 4$. However, these results might conflict with model predictions. The number density of faint galaxies is predicted to decrease right after the reionization ($z \simeq 6$; Becker et al. 2001), since the reionization increases the Jeans mass of the IGM and thus the minimum mass of forming galaxies (Gnedin & Ostriker 1997; Miralda-Escude & Rees 1998).

The average extinction of LBGs at z=4, $E(B-V)=0.15\pm0.03$, is the same as that of LBGs at z=3 derived by Adelberger & Steidel (2000) from their large sample of z=3 LBGs. Furthermore, the dependence of extinction on intrinsic luminosity for z=4 LBGs is similar to that for z=3 LBGs. This means that the average dust properties are the same between z=3 LBGs and z=4 LBGs. Interestingly, Ferguson, Dickinson, & Papovich (2002) find that most of the LBGs seen at z=3 started star formation after z=4, i.e., LBGs at z=3 are not descendants of LBGs at z=4. Thus, LBGs at z=3 and z=4 may be similarly young, and so have a similar amount of dust.

7.2. UV-Luminosity Density and Escape Fraction

We compare in Figure 21 the luminosity densities of LBGs at z = 4 - 5 in our samples with those at z = 3 and 4 which are calculated from the LFs given in Steidel et al. (1999). Figure 21 shows that the UV-luminosity density of LBGs does not change significantly from z = 3 to z = 5. The luminosity density of LBGs is $\rho_{\rm UV}^{\rm total} = 1.9 \pm 0.2 \times 10^{26}$, $2.0 \pm 0.2 \times 10^{26}$, and $1.6 \pm 0.7 \times 10^{26}$ erg s⁻¹ Hz⁻¹ Mpc⁻³ (see Table 4) for z = 3, z = 4, and z = 5, where the value at z = 4 is the mean of our measurement and Steidel et al.'s. Thus the ratio of the UV-luminosity density at z = 4 and 5 to that at z = 3 is $\rho_{\text{UV}}(z = 4)/\rho_{\text{UV}}(z = 3) = 1.0 \pm 0.2$ and $\rho_{\rm UV}(z=5)/\rho_{\rm UV}(z=3) = 0.8 \pm 0.4$. The total UVluminosity density may slightly decrease toward z = 5, but the amount of the decrease is 20% at most. Although the number density of bright LBGs $(M_{1700} \lesssim -22)$ significantly decreases toward z = 5 (Figure 16), the total UVluminosity density does not change largely. This is because the total UV-luminosity density is mainly contributed by LBGs fainter than $M_{1700} \sim -22$.

The luminosity density of LAEs at z=4.86 is calculated to be 9.6×10^{25} erg s⁻¹ Hz⁻¹ Mpc⁻³ with the UV-luminosity function obtained by SDS II in the same manner as for LBGs (Table 4). The ratio of the UV-luminosity density of LAEs to that of LBGs is $\rho_{\rm UV}({\rm LAE})/\rho_{\rm UV}({\rm LBG}) \simeq 0.6$ at $z\simeq5$. Since LBG samples are UV-luminosity limited samples (section 3.3), the UV-luminosity density derived from LBGs' LF represents the UV-luminosity density of the whole galaxy population (if an appropriate extrapolation of the LF down to a very faint luminosity is made). Thus, about 60% of the cosmic UV-luminosity density (or cosmic star-formation rate) at $z\sim5$ is contributed by galaxies identified as LAEs.

Figure 21 shows that the cosmic SFR is constant from $z\sim 1$ to $z\sim 5$. This result agrees with that obtained by Iwata et al. (2003), although the bright end of the luminosity function is significantly different between ours and Iwata et al.'s (2003). This coincidence indicates that faint LBGs ($SFR\sim 1h_{70}^{-2}M_{\odot}{\rm yr}^{-1}$) contribute much more to the cosmic SFR than bright LBGs ($SFR\gtrsim 100h_{70}^{-2}M_{\odot}{\rm yr}^{-1}$). The constant cosmic SFR from z=1-5 is consistent with predictions of numerical simulations. Ascasibar, Yepes, Gottlöber, & Müller (2002) have found from numerical simulations that the cosmic star-formation rate shows almost no drop over 2< z< 5, and that the star-formation is a gradual process with no characteristic epoch. Nagamine, Cen, & Ostriker (2000) have predicted from hydrodynamical simulations that the cosmic SFR shows a moderate plateau between z=1 and

z=3 and a gradual decrease beyond z=3 up to z=5 by ~ 0.4 dex. The cosmic SFR at z=3-5 is about 5 times larger than that at z=0 (top panel of Figure 21). The star-formation is very active at these high redshifts, but the accumulated stellar mass density (bottom panel of Figure 21) at z=3 is just 1/10 of the present-day stellar mass density. Since the cosmic time between z=5 and 3 is much shorter than that between z=3 and 0 (1Gyr versus 10Gyr), the majority of stars are produced not at these high redshifts (z=3-5) but at lower redshifts (z<3).

We calculate the number density of ionizing photons contributed by LBGs (section 6.2). We give a lower-limit for the escape fraction of ionizing photons for LBGs at $z=4.7~(f_{\rm esc}\gtrsim 0.13)$. It should be noted here that this $f_{\rm esc}$ value is inferred from a combination of the estimated UV-luminosity for LBGs and a model of ionization. In this sense, our method has intrinsically a large ambiguity, since most of the $f_{\rm esc}$ values given in the literature are based on direct measurements of the Lyman continuum in spectra (see below). Nevertheless, our results are useful, giving a new, independent constraint on $f_{\rm esc}$.

Steidel, Pettini, & Adelberger (2001) have found that the average spectrum of LBGs at $z \simeq 3.4$ has a Lyman continuum and that the flux ratio between the UV continuum at 1500Å and the Lyman continuum at 900Å is $f_{900}/f_{1500} = 1/4.6$ after correction for the IGM absorption. This flux ratio corresponds to an escape fraction, $f_{\rm esc} \sim 3 \times (1/4.6) = 0.65$, where the factor of 3 comes from the assumed shape of the intrinsic spectrum (see Giallongo, Cristiani, D'Odorico, & Fontana 2002). On the other hand, Giallongo, Cristiani, D'Odorico, & Fontana (2002) have found no Lyman-continuum flux in their two LBGs at z = 3, and they set an upper limit for the escape fraction of $f_{\rm esc} < 0.16$. The measurement of Giallongo, Cristiani, D'Odorico, & Fontana (2002) is not consistent with that of Steidel, Pettini, & Adelberger (2001). Giallongo, Cristiani, D'Odorico, & Fontana (2002) discuss that this inconsistency may be due to differences in sample selection. In either case, our estimate, $f_{\rm esc} \gtrsim 0.13$, is not seriously conflict with these two previous measurements, if the escape fraction does not change from z = 5 to z = 3. The escape fraction of LBGs is probably not smaller than

We compare these $f_{\rm esc}$ values with those of the present-day galaxies. Leitherer, Ferguson, Heckman, & Lowenthal (1995) have given an upper limit for four nearby starbursts using Far-UV spectra. The values they have obtained are $f_{\rm esc} \leq 0.0095, 0.017, 0.048,$ and 0.15. Hurwitz, Jelinsky, & Dixon (1997) re-analyzed the data of Leitherer, Ferguson, Heckman, & Lowenthal (1995) to obtain higher values: $f_{\rm esc} \leq 0.032, 0.052, 0.11,$ and 0.57. Tumlinson, Giroux, Shull, & Stocke (1999) have found $f_{\rm esc} \leq 0.02$ for NGC 3067. The escape fraction of the Milky Way Galaxy has been estimated to be $f_{\rm esc} \sim 0.06$ by Bland-Hawthorn & Maloney (1999). The average $f_{\rm esc}$ seems to be $f_{\rm esc} \lesssim 0.1$ for present-day galaxies. This implies that the escape fraction of LBGs at z=3-5 is larger than that of star-forming galaxies at z=0.

8. CONCLUSIONS

We have made large samples of 2,600 Lyman Break Galaxies (LBGs) at z=3.5-5.2 detected in deep ($i'\simeq 27$)

and wide-field (1,200 arcmin²) data of the Subaru Deep Field (SDF) and the Subaru/XMM Deep Field (SXDF), and have studied their photometric properties. The major findings of our study are summarized as follows.

- 1. We find that our selection criteria for LBGs can isolate about 90% of all galaxies in a targetted redshift range, if galaxies have sufficiently high S/N ratios (Figure 14 in section 3.3). Thus, our LBG samples are regarded as nearly UV-magnitude limited samples of high-z galaxies. The missed 10% galaxies are galaxies attenuated heavily by dust $(E(B-V) \gtrsim 0.4)$.
- 2. We derive luminosity functions of LBGs at $\langle z \rangle = 4.0$, 4.7, and 4.9 in section 4. We find no cosmic variance between the SDF and the SXDF. Then comparing them with that at $\langle z \rangle = 3$ (Steidel et al. 1999), we find that while the luminosity function of LBGs does not show a large change over z=3 and 4 as reported by Steidel et al. (1999), the number density of bright galaxies with $M_{1700} < -22$ (or galaxies with high star-formation rate of $SFR \gtrsim 100h_{70}^{-2}M_{\odot}~\rm yr^{-1}$ with extinction correction) decreases by an order of magnitude from z=4 to 5. We also find that the faint-end slope of the luminosity function may be steeper at z=4 than at z=3.
- 3. We estimate the dust extinction of LBGs at $z=4\pm0.5$ from the UV-continuum slope measured from i'-z' color (section 5). We do not measure dust extinction of LBGs at z>4.5, because i'-z' measurements are significantly affected by absorption of the IGM and by Ly α emission (Figure 18 of section 5.1). We find that LBGs with $M < M^*(\simeq -21)$ have $E(B-V) = 0.15 \pm 0.03$ on average if completeness correction is made to the sample, and that the amount of extinction depends not on apparent luminosity but on intrinsic luminosity. We find no evolution in dust extinction between z=3 and 4.
- 4. We calculate the UV-luminosity density at 1700Å for our LBGs by integrating the luminosity functions derived in section 4.1. Then we estimate the cosmic star-formation

rate at z=4 and z=5 from the UV-luminosity density, and compare them with those at z<4 given by various authors. We find that the UV-luminosity density at 1700Å, $\rho_{\rm UV}$, does not significantly change from z=3 to z=5, i.e., $\rho_{\rm UV}(z=4)/\rho_{\rm UV}(z=3)=1.0\pm0.2$ and $\rho_{\rm UV}(z=5)/\rho_{\rm UV}(z=3)=0.8\pm0.4$. Comparing the UV-luminosity density of LBGs at z=5 with that of Lyman α emitters (LAEs) at z=4.9 calculated from the data of SDS II, we obtain $\rho_{\rm UV}({\rm LAE})/\rho_{\rm UV}({\rm LBG})\simeq0.6$. It implies that about a half ($\simeq60\%$) of the star formation at $z\sim5$ occurs in LAEs.

- 5. We derive the cosmic star-formation rate (SFR) at $z \sim 4$ and 5 from $\rho_{\rm UV}$ of our LBGs (section 6.1) with correction for dust extinction of E(B-V)=0.15 obtained in section 5.2. Combining our measurements with those at $z \lesssim 3$ given in the literature, we find that the cosmic SFR is almost constant, or shows a possible decline, from z=3 to z=5. We then estimate the stellar mass density at $z \lesssim 5$ by integrating the cosmic SFR over time, and find that at $z \sim 1-3$ the stellar mass density based on the cosmic SFR exceeds that derived directly from the stellar mass function by a factor of 3, while the two estimates agree at $z \lesssim 1$.
- 6. We estimate the production rate of ionizing photons for LBGs from $\rho_{\rm UV}$ using the model proposed by Madau, Haardt, & Rees (1999) (section 6.2). We find that more than $\simeq 13\%$ of ionizing photons produced by massive stars should escape from LBGs at $z \simeq 5$ (i.e., $f_{\rm esc} \gtrsim 0.13$) in order to keep the IGM ionized.

We would like to thank the Subaru Telescope staff for their invaluable help in commissioning the Suprime-Cam that made these difficult observations possible. We thank the referee, Patrick McCarthy, for his constructive suggestions and comments that improved this article. M. Ouchi acknowledge support from the Japan Society for the Promotion of Science (JSPS) through JSPS Research Fellowships for Young Scientists.

REFERENCES

Adelberger, K. L. & Steidel, C. C. 2000, ApJ, 544, 218
Ascasibar, Y., Yepes, G., Gottlöber, S., & Müller, V. 2002, A&A, 387, 396
Baugh, C. M., Cole, S., Frenk, C. S., & Lacey, C. G. 1998, ApJ, 498, 504
Benítez, N. 2000, ApJ, 536, 571
Becker, R. H. et al. 2001, AJ, 122, 2850
Bertin, E. & Arnouts, S. 1996, A&AS, 117, 393
Bland-Hawthorn, J. & Maloney, P. R. 1999, ApJ, 510, L33
Brinchmann, J. & Ellis, R. S. 2000, ApJ, 536, L77
Bruzual A., G. & Charlot, S. 1993, ApJ, 405, 538
Bruzual A., G. & Charlot, S. MNRAS, submitted
Calzetti, D., Kinney, A. L. & Storchi-Bergmann, T. 1994, ApJ, 429, 582
Calzetti, D., Armus, L., Bohlin, R. C., Kinney, A. L., Koornneef, J., & Storchi-Bergmann, T. 2000, ApJ, 533, 682
Calzetti, D. 2001, PASP, 113, 1449
Chen, H. et al. 2003, ApJ, 586, 745
Cohen, J. G. 2002, ApJ, 567, 672
Cole, S. et al. 2001, MNRAS, 326, 255
Coleman, G. D., Wu, C.-C., & Weedman, D. W. 1980, ApJS, 43, 393
Connolly, A. J., Csabai, I., Szalay, A. S., Koo, D. C., Kron, R. G., & Munn, J. A. 1995, AJ, 110, 2655
Cowie, L. L., Songaila, A., Hu, E. M., & Cohen, J. G. 1996, AJ, 112, 839
Dickinson, M. 2000, Royal Society of London Philosophical Transactions Series A, 358, 2001 (astro-ph/0004028)

Dickinson, M., Papovich, C., Ferguson, H. C., & Budavári, T. 2003,

ApJ, 587, 25

Fan, X., Narayanan, V. K., Strauss, M. A., White, R. L., Becker, R. H., Pentericci, L., & Rix, H. 2002, AJ, 123, 1247
Ferguson, H. C., Dickinson, M., & Papovich, C. 2002, ApJ, 569, L65
Fernández-Soto, A. and Lanzetta, K. M. and Yahil, A. 1999, ApJ, 513, 34
Fontana, A., D'Odorico, S., Poli, F., Giallongo, E., Arnouts, S., Cristiani, S., Moorwood, A., & Saracco, P. 2000, AJ, 120, 2206
Franx, M. et al. 2003, ApJ, 587, L79
Fukugita, M., Shimasaku, K., & Ichikawa, T. 1995, PASP, 107, 945
Furusawa, H., Shimasaku, K., Doi, M., & Okamura, S. 2000, ApJ, 534, 624
Furusawa, H. 2002, Ph.D. Thesis, University of Tokyo
Gallego, J., Zamorano, J., Aragon-Salamanca, A., & Rego, M. 1995, ApJ, 455, L1
Giallongo, E., Cristiani, S., D'Odorico, S., & Fontana, A. 2002, ApJ, 568, L9
Glazebrook, K., Blake, C., Economou, F., Lilly, S., & Colless, M. 1999, MNRAS, 306, 843
Gnedin, N. Y. & Ostriker, J. P. 1997, ApJ, 486, 581
Gunn, J. E. & Stryker, L. L. 1983, ApJS, 52, 121
Gwyn, S. D. J. & Hartwick, F. D. A. 1996, ApJ, 468, L77
Hernquist, L. & Springel, V. 2003, MNRAS, 341, 1253
Hu, E. M., Cowie, L. L., McMahon, R. G., Capak, P., Iwamuro, F., Kneib, J.-P., Maihara, T., & Motohara, K. 2002, ApJ, 568, L75
Hurwitz, M., Jelinsky, P., & Dixon, W. V. D. 1997, ApJ, 481, L31
Iwata, I., Ohta, K., Tamura, N., Ando, M., Wada, S., Watanabe, C., Akiyama, M., & Aoki, K. 2003, PASJ, 55, 415
Kashikawa, N. et al. 2002, PASJ, 54, 819

Kashikawa, N. et al. 2003, AJ, 125, 53 (SDS III)

Kauffmann, G., Colberg, J. M., Diaferio, A., & White, S. D. M. 1999, MNRAS, 307, 529

Kodaira, K. et al. 2003, PASJ, 55, L17

Labbé, I. et al. 2003, AJ, 125, 1107 Landolt, A. U. 1992, AJ, 104, 340

Lanzetta, K. M., Yahil, A., & Fernandez-Soto, A. 1996, Nature, 381,

Le Fevre, O., Hudon, D., Lilly, S. J., Crampton, D., Hammer, F., & Tresse, L. 1996, ApJ, 461, 534

Leitherer, C., Ferguson, H. C., Lowenthal, J. D. et al. 1997, ApJ, 481, 673

Madau, P. 1995, ApJ, 441, 18 Madau, P., Ferguson, H. C., Dickinson, M. E., Giavalisco, M., Steidel,

C. C., & Fruchter, A. 1996, MNRAS, 283, 1388 Madau, P., Pozzetti, L., & Dickinson, M. 1998, ApJ, 498, 106 Madau, P., Haardt, F., & Rees, M. J. 1999, ApJ, 514, 648 Maihara, T. et al. 2001, PASJ, 53, 25 (SDS I)

Massarotti, M., Iovino, A., Buzzoni, A., & Valls-Gabaud, D. 2001,

A&A, 380, 425

Meurer, G. R., Heckman, T. M., & Calzetti, D. 1999, ApJ, 521, 64 Miralda-Escude, J. & Rees, M. J. 1998, ApJ, 497, 21

Miyazaki, S. et al. 2002, PASJ, 54, 833 Monet, D. E. A. 1998, The PMM USNO-A2.0 Catalog.

Motohara, K. et al. 2002, PASJ, 54, 315

Nagamine, K., Cen, R., & Ostriker, J. P. 2000, ApJ, 541, 25

Oke, J. B. 1974, ApJS, 27, 21 Oke, J. B. 1990, AJ, 99, 1621

Ouchi, M., Yamada, T., Kawai, H., & Ohta, K. 1999, ApJ, 517, L19 Ouchi, M. et al. 2001, ApJ, 558, L83 Ouchi, M. et al. 2003a, ApJ, 582, 60 (SDS II) Ouchi, M. 2003b, Ph.D. Thesis, University of Tokyo

Ouchi, M. 2003c, submitted to ApJ (astro-ph/0309657) (SDS VI) Papovich, C., Dickinson, M., & Ferguson, H. C. 2001, ApJ, 559, 620 Pascarelle, S. M., Windhorst, R. A., & Keel, W. C. 1998, AJ, 116,

Pettini, M., Kellogg, M., Steidel, C. C., Dickinson, M., Adelberger, K. L. & Giavalisco, M. 1998, ApJ, 508, 539
Pettini, M., Shapley, A. E., Steidel, C. C., Cuby, J., Dickinson, M., Moorwood, A. F. M., Adelberger, K. L., & Giavalisco, M. 2001, ApJ, 554, 981

Pettini, M., Rix, S. A., Steidel, C. C., Adelberger, K. L., Hunt, M. P., & Shapley, A. E. 2002, ApJ, 569, 742

Poli, F., Menci, N., Giallongo, E., Fontana, A., Cristiani, S., & D'Odorico, S. 2001, ApJ, 551, L45

Rudnick, G. et al. 2001, AJ, 122, 2205

Sawicki, M. J., Lin, H., & Yee, H. K. C. 1997, AJ, 113, 1

Sawick, M., & Yee, H. K. C. 1998, AJ, 115, 1329

Schechter, P. 1976, ApJ, 203, 297

Schlegel, D. J., Finkbeiner, D. P., & Davis, M. 1998, ApJ, 500, 525

Shapley, A. E., Steidel, C. C., Adelberger, K. L., Dickinson, M., Giavalisco, M., & Pettini, M. 2001, ApJ, 562, 95

Shimasaku, K. et al. 2003, ApJ, 586, L111 (SDS IV)

Shimasaku, K. et al. 2003, ApJ, 586, L111 (SDS IV) Spergel, D. N. et al. 2003, ApJ in press, (astro-ph/0302209)

Steidel, C. C., Giavalisco, M., Pettini, M., Dickinson, M., & Adelberger, K. L. 1996a, ApJ, 462, L17
Steidel, C. C., Giavalisco, M., Dickinson, M., & Adelberger, K. L.

1996b, AJ, 112, 352 Steidel, C. C., Adelberger, K. L., Giavalisco, M., Dickinson, M., & Pettini, M. 1999, ApJ, 519, 1

Steidel, C. C., Pettini, M., & Adelberger, K. L. 2001, ApJ, 546, 665 Steidel, C. C., Hunt, M. P., Shapley, A. E., Adelberger, K. L., Pettini, M., Dickinson, M., & Giavalisco, M. 2002, ApJ, 576, 653

Steidel, C. C., Adelberger, K. L., Shapley, A. E., Pettini, M., Dickinson, M., & Giavalisco, M. 2003, ArXiv Astrophysics e-prints, 5378 (astro-ph/0305378)

Sullivan, M., Treyer, M. A., Ellis, R. S., Bridges, T. J., Milliard, B., & Donas, J.; 2000, MNRAS, 312, 442

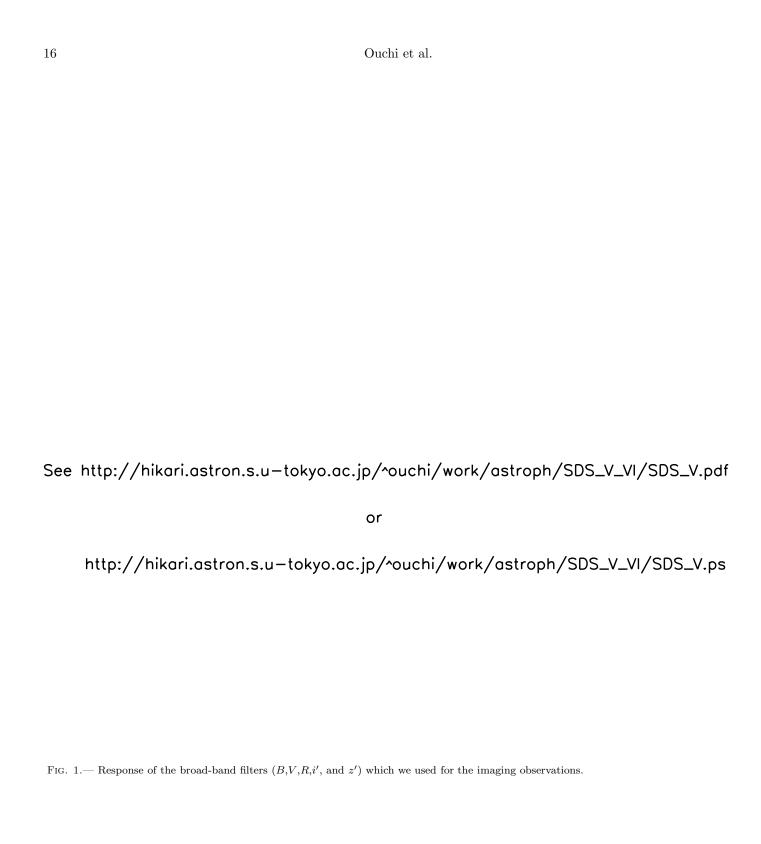
Tresse, L. & Maddox, S. J. 1998, ApJ, 495, 691 Tumlinson, J., Giroux, M. L., Shull, J. M., & Stocke, J. T. 1999, AJ, 118, 2148

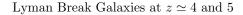
Vijh, U. P., Witt, A. N., & Gordon, K. D. 2003, ApJ, 587, 533 Wang, Y., Bahcall, N., & Turner, E. L. 1998, AJ, 116, 2081

Weinberg, D. H., Hernquist, L., & Katz, N. 2002, ApJ, 571, 15 Yagi, M., Kashikawa, N., Sekiguchi, M., Doi, M., Yasuda, N., Shimasaku, K., & Okamura, S. 2002, AJ, 123, 66

Yahata, N., Lanzetta, K. M., Chen, H., Fernández-Soto, A., Pascarelle, S. M., Yahil, A., & Puetter, R. C. 2000, ApJ, 538,

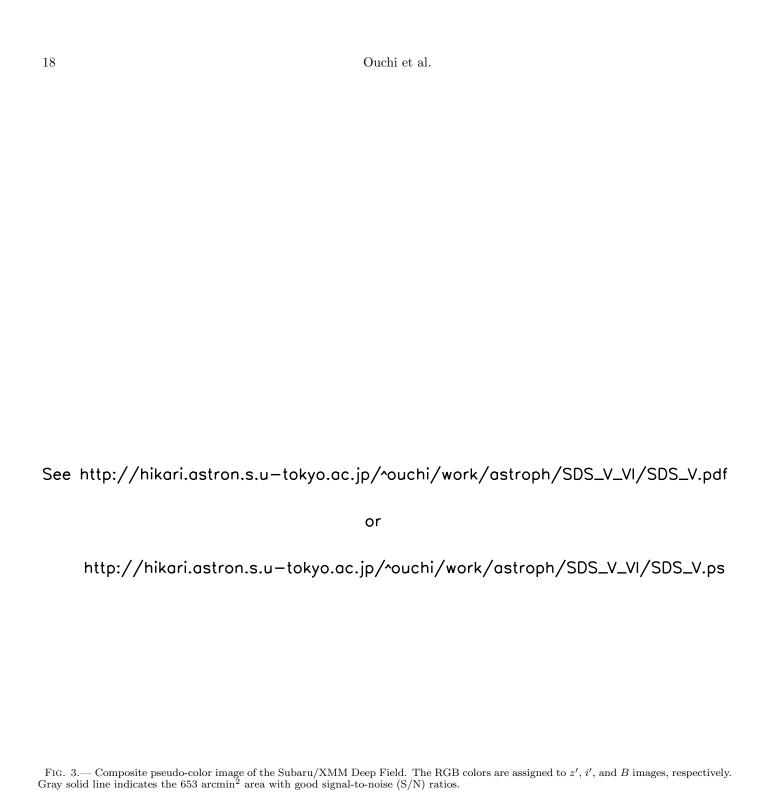
Yan, L., McCarthy, P. J., Freudling, W., Teplitz, H. I., Malumuth,
E. M., Weymann, R. J., & Malkan, M. A. 1999, ApJ, 519, L47
Yan, H., Windhorst, R. A., & Cohen, S. H. 2003, ApJ, 585, L93





or

Fig. 2.— Composite pseudo-color image of the Subaru Deep Field. The RGB colors are assigned to z', i', and B images, respectively. The square outlined by the white line near the center of the image is the field where deep near-infrared J and K images have been obtained by Subaru/CISCO (SDS I). A magnified image of this field is shown in the upper right panel. Gray solid line indicates the 616 arcmin² area with good signal-to-noise (S/N) ratios in all bands except for the R band. We use this area for detecting Viz-LBGs. Gray dashed line corresponds to the border of good and bad S/N regions in the R band. The R band data do not have good S/N below the gray dashed line, and we use the remaining 543 arcmin² field for detecting BRi-LBGs and Riz-LBGs. The 543 arcmin² field is also the field where we detect 87 LAEs at z=4.86 as described in SDS II.





or

http://hikari.astron.s.u-tokyo.ac.jp/^ouchi/work/astroph/SDS_V_VI/SDS_V.ps

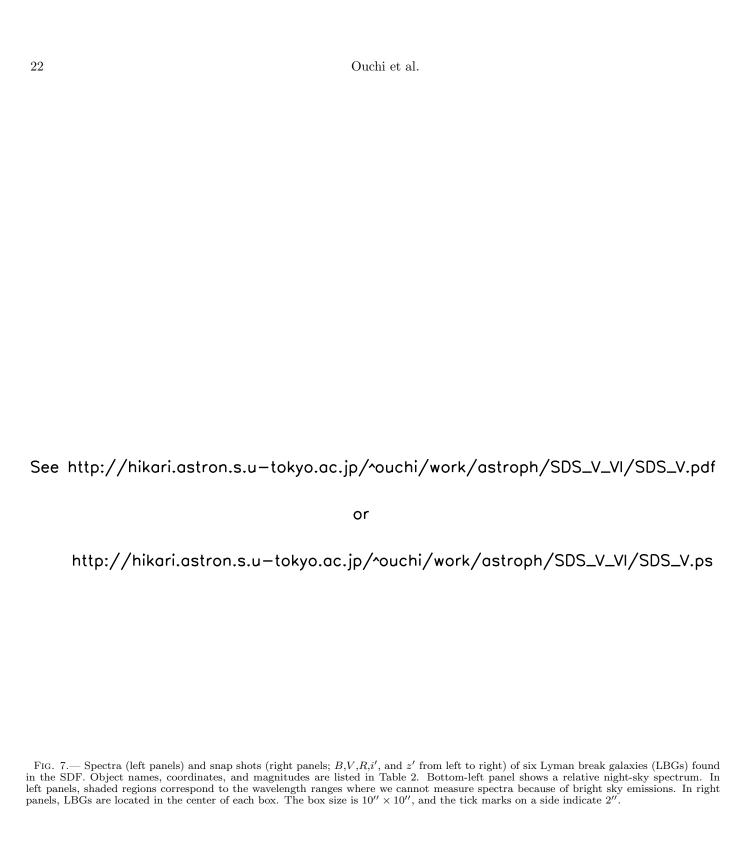
Fig. 4.— Left panel: B-R vs. R-i' color diagram displaying the colors of model galaxies and stars. Red line shows the track of a typical spectrum of star-forming galaxies from z=3 to 4. The typical spectrum is produced by the GISSEL00 (Bruzual & Charlot 2003) population synthesis model with the same parameters as for the average $z\simeq 3$ galaxy (Papovich, Dickinson, & Ferguson 2001): Salpeter IMF, $Z=0.2Z_{\odot}$, and 70 Myr passed from the initial star formation with Calzetti's (Calzetti et al. 2000) dust attenuation of E(B-V)=0.16. Filled circles on the red line indicate the redshift from z=3.3 to z=3.9 with an interval of $\Delta z=0.1$. Typical spectra of elliptical, Sbc, Scd, and irregular galaxies taken from Coleman, Wu, & Weedman (1980) are redshifted from z=0 to z=3, which are shown by green, cyan, blue, and violet lines, respectively. Each line is marked by filled circles at z=0,1, and 2. Yellow star marks are 175 Galactic stars given by Gunn & Stryker (1983). Right panel: B-R vs. R-i' color diagram displaying the colors of 1048 HDF-N photo-z galaxies obtained by convolution of their best-fit SEDs (Furusawa et al. 2000) with the filter transmissions of Suprime-Cam. Black and red dots indicate galaxies whose photometric redshifts are $0 < z \le 3$ and z > 3, respectively.

or

Fig. 5.— Same as Figure 4, but for V-i' vs. i'-z'. Filled circles on the red line in the left panel indicate the redshift from z=3.9 to z=4.7 with an interval of $\Delta z=0.1$.

or

Fig. 6.— Same as Figure 4, but for R-i' vs. i'-z'. Filled circles on the red line in the left panel indicate the redshift from z=4.5 to z=5.3 with an interval of $\Delta z=0.1$.



or

http://hikari.astron.s.u-tokyo.ac.jp/^ouchi/work/astroph/SDS_V_VI/SDS_V.ps

FIG. 8.— Upper panels: B-R vs. R-i' color diagram displaying the probability maps of low-z interlopers and high-z galaxies in the SDF (left panel) and SXDF (right panel). The probability is estimated by Monte Carlo simulations using best-fit SEDs of galaxies in the HDF-N photometric-redshift catalog (Furusawa et al. 2000). Red and yellow contours show the probabilities of high-z galaxies in a bright magnitude bin (i'=23.5-24.0 for both fields) and a faint magnitude bin (i'=26.0-26.5 for SDF, i'=25.5-26.0 for SXDF), respectively. Four contour levels are 50%, 70%, 90% and 95% (from edge to center) of the source completeness, respectively. The probability map of faint galaxies (yellow contours) is generally wider than that of bright galaxies (red contours), since fainter galaxies have larger photometric errors. The contours for the faint galaxies do not extend to large B-R, because of a limited depth of the B-band data. Blue contours show the probabilities of low-z contaminants integrated over i'<26.5. Their four contour levels are 0.5%, 1.0%, 5.0%, and 10% (from edge to center) of all the contaminants in a unit area (mag²; i.e., $\Delta(B-R)=1$ and $\Delta(R-i')=1$). Green line indicates the selection criteria of BRi-LBGs. Red and blue circles indicate 85 spectroscopically identified objects which are located at high redshift (3.5 < z < 4.5) and at low redshift (0 < z ≤ 3.5), respectively. Red triangle denotes an object located at high redshift (3.5 < z < 4.5) but whose B-band magnitude is below the 1σ magnitude. Lower panels: B-R vs. R-i' colors of objects in our SDF catalog (left panel: 45,923 objects with i' < 26.5) and SXDF catalog (right panel: 39,301 objects with i' < 26.0). A dot indicates an object. If the magnitude of an object is fainter than the 1σ magnitude (1σ sky fluctuation), then the magnitude is replaced with the 1σ magnitude. This replacement produces artificial sequences in the two-color diagram around (R-i', B-R) = (1.5, 1.0) and (2.0,0.7) for the

 $See \ http://hikari.astron.s.u-tokyo.ac.jp/\verb|^ouchi/work/astroph/SDS_V_VI/SDS_V.pdf| \\$

or

 $http://hikari.astron.s.u-tokyo.ac.jp/\verb|^ouchi/work/astroph/SDS_V_VI/SDS_V.ps|$

FIG. 9.— Upper panels: Same as the upper panels of Figure 8, but for V-i' vs. i'-z'. Red and yellow contours show the probabilities of high-z galaxies in a bright magnitude bin (z'=24.0-24.5 for both fields) and a faint magnitude bin (z'=25.5-26.0 for SDF, z'=25.0-25.5 for SXDF), respectively. Green solid lines indicate the selection criteria of Viz-LBGs for the SDF data. Green dotted line in the right panel shows the criteria of Viz-LBG for the SXDF data (eq. 4). Red and blue circles indicate 85 spectroscopically identified objects which are located at high redshift (4.2 < z < 5.2) and at low redshift ($0 < z \le 4.2$), respectively. Two red points far below the selection criteria denote galaxies at z=4.250 and z=4.270. Since the selection criteria of Viz-LBGs have a completeness of just $\sim 20\%$ for these redshifts, it is consistent that the colors of these two galaxies are well separated from the selection criteria. These two galaxies are selected by the criteria for BRi-LBGs. Lower panels: Same as the lower panels of Figure 8, but for V-i' vs. i'-z' colors of objects in our SDF catalog (left panel: 37,486 objects with z' < 26.0) and SXDF catalog (right panel: 34,024 objects with z' < 25.5). A dot indicates an object. If the magnitude of an object is fainter than the 1σ magnitude (1σ sky fluctuation), then the magnitude is replaced with the 1σ magnitude. This replacement produces artificial sequences in the two-color diagram around (i'-z', V-i') = (1.5, 1.3) and (2.2, 0.4) for the SDF, and (i'-z', V-i') = (1.5, 0.9) and (2.0, 0.3) for the SXDF. Green solid lines indicate the selection criteria of Viz-LBGs for the SDF data. Green dotted line in right panel shows the criteria of Viz-LBG for the SXDF data (eq. 4).

or

 $http://hikari.astron.s.u-tokyo.ac.jp/\verb|^ouchi/work/astroph/SDS_V_VI/SDS_V.ps| \\$

Fig. 10.— Upper panels: Same as the upper panels of Figure 8, but for R-i' vs. i'-z'. Red and yellow contours show the probabilities of high-z galaxies in a bright magnitude bin (z'=24.0-24.5 for both fields) and a faint magnitude bin (z'=25.5-26.0 for SDF, z'=25.0-25.5 for SXDF), respectively. Green lines indicate the selection function of Riz-LBGs. Red and blue circles indicate 85 spectroscopically identified objects which are located at high redshift (4.6 < z < 5.2) and at low redshift ($0 < z \le 4.2$), respectively. The red point denotes a galaxy at z=4.865. This galaxy is not included in the Riz-LBG sample (probably due to its photometric errors), but this galaxy is identified by the selection criteria of Viz-LBGs. Lower panels: Same as the lower panels of Figure 8, but R-i' vs. i'-z' colors of objects in our SDF catalog (left panel: 37,486 objects with z' < 26.0) and SXDF catalog (right panel: 34,024 objects with z' < 25.5). A dot indicates an object. If the magnitude of an object is fainter than the 1σ magnitude (1σ sky fluctuation), then the magnitude is replaced with the 1σ magnitude. This replacement produces artificial sequences in the two-color diagram around (i'-z', R-i') = (1.5, 1.0) and (2.2, 0.2) for the SDF, and (i'-z', R-i') = (2.0, 1.0) and (2.0, 0.0). for the SXDF. Green lines indicate the selection criteria of Riz-LBGs.

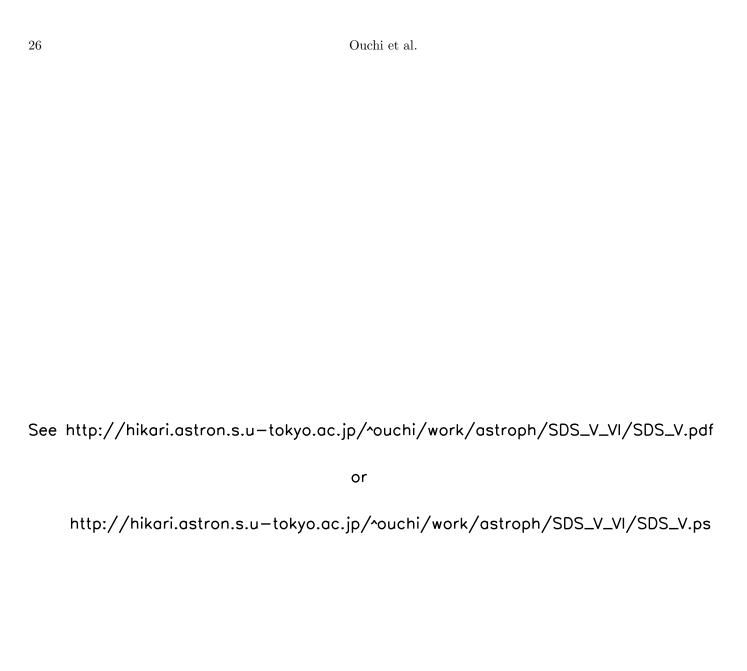


Fig. 11.— Number counts of the LBGs selected in the SDF and SXDF. BRi-LBGs, Viz-LBGs, and Riz-LBGs are shown separately. Magnitude, $m_{\rm AB}$, is i'-band magnitude for BRi-LBGs and z'-band magnitude for Viz-LBGs and Riz-LBGs. Filled circles and filled squares are data from the SDF and SXDF, respectively. Since the selection criteria for Viz-LBGs are different between the SDF and the SXDF, we do not plot data for Viz-LBGs in the SXDF to avoid confusion. Open squares (top panel) and triangles (middle panel) indicate measurements for LBGs at $z \simeq 4$ and 5 obtained by Steidel et al. (1999) and Iwata et al. (2003), respectively. The number counts of our LBGs at $z \sim 4$ agree well with those of Steidel et al.'s, while for Viz-LBGs a large discrepancy is seen at bright magnitudes between our measurements and Iwata et al.'s. See text for more details.

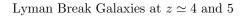


or

FIG. 12.— Completeness as a function of redshift for our LBG samples. In the panels of BRi-LBGs, thin solid, dotted, dot-dashed, and dashed lines denote the completeness for BRi-LBGs with $i' = -\infty, 24.25, 25.25, 26.25$ ($i' = -\infty, 23.75, 24.75, 25.75$,) in the SDF (SXDF). In the panels of Viz-LBGs and Riz-LBGs, thin sold, dot-dashed, and dashed lines denote the completeness for Viz-LBGs and Riz-LBGs with $z' = -\infty, 24.75, 25.75$ ($z' = -\infty, 24.25, 25.25$) in the SDF (SXDF). Thick solid lines plotted in all panels show number-wighted completeness, which is calculated by averaging the magnitude-dependent completeness weighted by the number of selected LBGs in each magnitude bin ($\Delta m = 0.5$). Since tighter selection criteria (eq. 4) are applied to Viz-LBGs in the SXDF, their selection window is narrower than that of Viz-LBGs in the SDF. Note that the peak sensitivity of the Riz-LBG selection is at a slightly lower redshift than that of the Viz-LBG selection. This is because we have set a tighter selection boundary near the high-z end ($z \simeq 5$) in the Riz-LBG selection than in the Viz-LBG selection to avoid interlopers, since galaxies near z = 5 have colors in R - i' and i' - z' close to low-z interlopers (Figures 6 and 10).



for Viz-LBGs and Riz-LBGs.



or

Fig. 14.— Redshift distribution of galaxies in (Furusawa et al. 2000)'s HDF-N photometric redshift catalog. In all panels, open histograms are for all galaxies in the catalog. Filled histograms are for galaxies which satisfy at least one of our BRi-, Viz-, or Riz-LBG selections (top panel), BRi-LBG selection (second panel), Viz-LBG selection (third panel), and Riz-LBG selection (bottom panel), respectively. The top panel indicates that at z=3.9-5.1, four out of the 47 galaxies escape from our LBG selections.

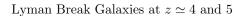




or

FIG. 16.— Luminosity functions (LFs) of LBGs at z=4-5. LFs of BRi-, Viz-, and Riz-LBGs are given in top panel, middle panel, and bottom panel, respectively. In each panel, filled circles (open circles) are the LFs derived from the SDF (SXDF) data. Solid lines are the best-fit Schechter function whose parameters are shown in Table 4 (see text). Dashed lines denote the LF of UV-selected galaxies in the local universe (Sullivan et al. 2000), while dotted lines are the LF of LBGs at $z\simeq 3$ derived by Steidel et al. (1999). In the top panel, the best-fit Schechter function of LBGs at z=4 (Steidel et al. 1999) is shown by the dash-long dashed line down to ~ -21 mag. Steidel et al. (1999) measured the LF down to ~ -21 mag with their wide-field LBG survey and fitted the Schechter function with a fixed slope ($\alpha=-1.6$). The upper abscissa axis, $SFR_{\rm raw}$, indicates the star-formation rate without extinction correction, which is converted from M_{1700} using eq. (12). The true (extinction-corrected) star-formation rate is about a factor of 4 larger than the raw rate. See text for details.





or

FIG. 18.— Redshift dependence of the E(B-V)- β_{iz} relationship calculated from the template model. Solid line is the relation for LBGs at z=4, and dashed and dot-dashed lines are for z=3.5 and z=4.5, respectively. The difference in the relation for LBGs at z=3.5-4.5 is less than ± 0.05 mag in E(B-V) for LBGs with $E(B-V) \le 0.5$. The upper and lower dotted lines are the relation of LBGs at z=4.7 and z=5.2, respectively.



or

Fig. 19.— Histograms of E(B-V) for four different magnitude bins for BRi-LBGs in the SDF and SXDF. Top panel shows the completeness of our LBG detection obtained by a simulations. In the top panel, the solid line is the histogram of input objects for the simulation. Dotted, dashed, dot-dashed, and long-dashed lines are the completeness of LBGs with i'=23.75,24.25,24.75, and 25.25, respectively. Second top to bottom panels show the number of objects in each magnitude bin as a function of extinction. In these panels, shaded histograms correspond to measurements corrected for the completeness shown in the top panel, while open histograms show raw numbers. Arrows denote the mean value of extinction calculated from the shaded histogram for each bin. Since the completeness for objects with large extinction values, E(B-V)>0.55, is less than 20%, we do not include those objects in the calculation of the mean value.



or

Fig. 20.— Histograms of E(B-V) for galaxies at z=0, 3, and 4. Shaded histogram in the top panel shows the distribution of local starburst galaxies derived from IUE data (Meurer, Heckman, & Calzetti 1999), while the shaded histogram in the middle panel is for LBGs at z=3 (Adelberger & Steidel 2000). Dotted histogram in the bottom panel presents our BRi-LBGs (z=4 LBGs) without correction for completeness. The open histogram in each panel shows the distribution of completeness-corrected BRi-LBGs down to i'=25 (or $M\simeq M^*$). Arrows indicate the mean values of extinction for galaxies at each redshift, which are calculated from the data over $0.0 \le E(B-V) \le 0.5$ for a fair comparison. Contamination-corrected data are used for the calculation for our BRi-LBGs and LBGs at z=3.

See http://hikari.astron.s.u-tokyo.ac.jp/^ouchi/work/astroph/SDS_V_VI/SDS_V.pdf

٥r

http://hikari.astron.s.u-tokyo.ac.jp/^ouchi/work/astroph/SDS_V_VI/SDS_V.ps

Fig. 21.— Top panel: Cosmic star-formation rate (SFR) as a function of redshift. The cosmic SFR is calculated from the luminosity density at $\simeq 2000 \text{Å}$, $\rho_{2000}^{\text{corr}}$, estimated from $\rho_{\text{UV}}^{\text{obs}}$ which are corrected for dust extinction of E(B-V)=0.15 whose value is indicated by a long arrow (see section 5). Circles, squares, diamonds, and stars are values for LBGs at z=4-5 (present study), LBGs at z=3-4 (Steidel et al. 1999), galaxies at $z \sim 1$ (Cowie, Songaila, Hu, & Cohen 1996), and galaxies at $z \simeq 0$ (Sullivan et al. 2000), respectively. Filled symbols indicate the total cosmic SFRs calculated by integrating the luminosity functions down to $L=0.1L^*$, and open symbols with arrows show lower limits, i.e., contributions only by actually detected galaxies. Differences between filled symbols and open symbols are due to the contributions from faint galaxies below the detection limits. Open triangles plotted at z>3 indicate the upper limits which are calculated by integrating the luminosity functions down to L=0. Pluses at z=0, 0.2, 0.9, and 1.3 are cosmic SFRs derived from the H α luminosity density (Gallego, Zamorano, Aragon-Salamanca, & Rego 1995, Tresse & Maddox 1998, Glazebrook et al. 1999, and Yan et al. 1999, respectively). Note that the cosmic SFRs estimated from $\rho_{2000}^{\text{corr}}$ (filled symbols) are comparable to those calculated from the H α luminosity density (pluses) at z=0-1. The shaded region shows approximated evolution of cosmic SFR obtained from fit of an analytic function (see text for details) to the data points. Bottom panel: Stellar mass density as a function of redshift. The shaded region indicates the stellar mass density calculated from the cosmic SFR shown as the shaded region in the top panel. Dashed line shows the stellar mass density calculated from the cosmic SFR observed galaxies alone (i.e., open symbols in the top panel). Filled circles, squares, and diamonds denote the stellar mass density derived from the stellar mass function by Cole et a



or

Fig. 22.— UV-ionizing photon density $(\dot{N}_{\rm ion})$ of the universe at z=2-5. Solid line indicates $\dot{N}_{\rm ion}$ required to maintain the ionization of the IGM predicted by Madau, Haardt, & Rees (1999). Dashed line is $\dot{N}_{\rm ion}$ contributed from QSOs. Diamond and circles denote the sum of the ionizing photons from QSOs and galaxies, where the ionizing photons from galaxies are estimated from LBGs at z=3 (Steidel et al. 1999) and at z=4 and 5 (present data) assuming $f_{\rm esc}=0.13$. This figure visualizes the fact that the average $f_{\rm esc}\gtrsim 0.13$ is required for galaxies at z=4.7 in order to maintain ionization.

Table 1
Journal of Observations

Field Name	Band	Observed dates	Area (arcmin)	Total Exposure Time (min)	$m_{ m lim}$
SDF	B	2001 Apr 24-25, May 20	616	210	27.8
SDF	V	2001 Apr 23, May 20	616	150	27.3
SDF	R	2001 Mar 21-23	543	90	27.1
SDF	i'	2001 Apr 24, Mar 19, Jun 23-24	616	138	26.9
$_{ m SDF}$	z'	2001 May 19-20, Jun 25	616	81	26.1
SXDF	B	2000 Nov 24-25	653	177	27.6
SXDF	V	2000 Nov 26-27	653	84	26.5
SXDF	R	2000 Nov 22,24, 2001 Nov 16	653	118	27.2
SXDF	i'	2000 Nov 25	653	45	26.2
SXDF	z'	2001 Oct 14,18,19	653	40	25.7

Note. — These data were taken in 2000 and 2001 during the GTOs of Suprime-Cam. Although deeper imaging (3-10 hours for each band) was carried out for both fields in 2002 and 2003 by the Subaru Observatory key projects (e.g., Kodaira et al. 2003; see section 1), the results presented in this paper are based on the GTO data only.

 ${\it Table \ 2}$ Lyman break galaxies with spectroscopic redshifts

Object Name	RA(J2000)	Dec(J2000)	z	B	V	R	i'	z'
SDFJ132410.8+272758 SDFJ132413.3+274207 SDFJ132416.3+274355 SDFJ132413.1+274116 SDFJ132411.4+273016	13:24:10.8 13:24:13.3 13:24:16.3 13:24:13.1 13:24:11.4	+27:27:58 +27:42:07 +27:43:55 +27:41:16 +27:30:16	3.845 4.140 4.250 4.270 4.600	27.79 27.84 > 29.0 > 29.0 > 29.0	26.21 26.10 25.54 27.32 26.61	25.09 25.32 24.54 26.08 25.40	25.00 25.16 24.09 26.10 24.66	24.97 25.17 24.02 25.91 24.51
SDFJ132410.5+274254	13:24:10.5	+27:42:54	4.865	> 29.0	> 28.5	27.21	25.96	25.98

Note. — Magnitudes are $2^{\prime\prime}\phi$ aperture magnitudes.

 $\begin{tabular}{ll} Table 3 \\ Photometric Samples of Galaxies \\ \end{tabular}$

Field Name	Sample Name	Detection Band	Number	Magnitude Range [‡]	Selection Criteria
SDF	$BRi ext{-}\mathrm{LBG}$	i'	1,438	i' = 23.5 - 26.5	eq. (1)
SDF	$Viz\text{-}\mathrm{LBG}$	z'	246	z' = 24.0 - 26.0	eq. (2)
SDF	$Riz\text{-}\mathrm{LBG}$	z'	68	z' = 24.0 - 26.0	eq. (3)
SXDF	$BRi\text{-}\mathrm{LBG}$	i'	732	i' = 23.5 - 26.0	eq. (1)
SXDF	$Viz\text{-}\mathrm{LBG}$	z'	34^{\dagger}	i' = 23.5 - 25.5	eq. (4)
SXDF	$Riz ext{-}\mathrm{LBG}$	z'	38	i' = 24.0 - 25.5	eq. (3)

 $^{^{\}ddagger}2^{\prime\prime}\phi$ aperture magnitudes.

 $^{^{\}dagger}Viz\text{-LBGs}$ of the SXDF are selected by the equation 4.

Table 4
Summary of the luminosity functions.

Sample Name	z	$\phi^* (h_{70}^3 \text{Mpc}^{-3})$	$\begin{array}{c} M_{1700}^* \\ (\mathrm{mag}) \end{array}$	α	$n^{\text{obs}\dagger} (h_{70}^3 \text{Mpc}^{-3})$	$\begin{array}{c} \rho_{\mathrm{UV}}^{\mathrm{obs}\dagger} \\ (\mathrm{erg}\ \mathrm{s}^{-1}\ \mathrm{Hz}^{-1}) \end{array}$	$(\operatorname{erg}\operatorname{s}^{-1}\operatorname{Hz}^{-1})$
BRi-LBG	$4.0^{+0.5}_{-0.5}$	$1.2 \pm 0.2 \times 10^{-3}$	-21.0 ± 0.1	-2.2 ± 0.2	$2.0 \pm 0.3 \times 10^{-3}$	$1.2 \pm 0.2 \times 10^{26}$	$2.9 \pm 0.4 \times 10^{26}$
$Viz\text{-}\mathrm{LBG}$	$4.7^{+0.5}_{-0.5}$	$1.4 \pm 0.8 \times 10^{-3}$	-20.7 ± 0.2	-2.2(fix)	$2.8 \pm 1.7 \times 10^{-4}$	$2.7 \pm 1.8 \times 10^{25}$	$2.4 \pm 1.4 \times 10^{26}$
$Riz ext{-}\mathrm{LBG}$	$4.9^{+0.3}_{-0.3}$	$\simeq 6.4 \times 10^{-4}$					$\simeq 1.1 \times 10^{26}$
BRi-LBG	$4.0^{+0.5}_{-0.5}$						$2.4 \pm 0.2 \times 10^{26} \ (4.3 \pm 0.3 \times 10^{26})$
$Viz\text{-}\mathrm{LBG}$	$4.7^{+0.5}_{-0.5}$	$2.4 \pm 1.0 \times 10^{-3}$	-20.3 ± 0.2	-1.6(fix)	$2.7 \pm 1.2 \times 10^{-4}$	$2.7 \pm 1.3 \times 10^{25}$	$1.6 \pm 0.7 \times 10^{26} \ (2.9 \pm 1.2 \times 10^{26})$
$Riz\text{-}\mathrm{LBG}$	$4.9^{+0.3}_{-0.3}$	$\simeq 1.0 \times 10^{-3}$	-20.3(fix)	-1.6(fix)	$\simeq 1.1 \times 10^{-4}$		$\simeq 7.0 \times 10^{25} \ (\simeq 1.2 \times 10^{26})$
LAE^{\ddagger}	$4.86^{+0.03}_{-0.03}$	1.9×10^{-3}	-20.0	-1.6(fix)	1.5×10^{-3}	5.0×10^{25}	9.6×10^{25}

 $^{^\}dagger$ Number density $(n^{\rm obs})$ and luminosity density $(\rho^{\rm obs}_{\rm UV})$ down to the observed limiting magnitudes; $M_{1700}=-19.8~(i'_{\rm ap}=26.5)$ for $BRi\text{-LBGs},~M_{1700}=-20.5~(z'_{\rm ap}=26.0)$ for $Viz\text{-LBGs},~M_{1700}=-20.5~(z'_{\rm ap}=26.0)$ for Riz-LBGs, and $M_{1700}=-19.03~(i'_{\rm ap}=27.5)$ for LAEs, where $i'_{\rm ap}$ and $z'_{\rm ap}$ are 2" ϕ aperture magnitudes in i' and z', respectively, and M_{1700} is rest-frame 1700Å absolute magnitude after aperture correction and k-correction (see text for details).

^{††} Total luminosity density ($\rho_{\text{UV}}^{\text{total}}$) calculated by integrating the luminosity function down to $L=0.1L^*$ assuming $\alpha=-2.2$ or -1.6. Values in parentheses are upper limits which are calculated by integrating the luminosity function down to L=0 assuming $\alpha=-1.6$.

[‡] Lyman α emitters at $z=4.86\pm0.03$ obtained by SDS II. We use the best-fit UV-lumonisity function given in SDS II to calculate the UV-luminosity density.

Note. — We refer to the values of BRi-LBGs and Viz-LBGs as those of z=4 and z=5 LBGs, since the values for Riz-LBGs are quite uncertain. In sections 6.1 and 6.2, we use values obtained for $\alpha=-1.6$.